

Use of Superconducting Magnet Technology for Astronaut Radiation Protection

Massachusetts Institute of Technology
Cambridge, Massachusetts

2 May, 2005

Final Report for NIAC Phase I Contract CP 04-01

Principal Investigator: Jeffrey A. Hoffman
Professor of the Practice of Aerospace Engineering
Co-Investigator: Peter Fisher
Professor of Physics
Researcher: Oleg Batishchev
Principal Research Scientist, Aero/Astro Dept.

Abstract

Left unshielded, astronauts on long, interplanetary voyages will be exposed to dangerous doses of radiation from cosmic rays. The proposed superconducting magnetic radiation shielding system could reduce the mass of shielding required for interplanetary travel compared to traditional absorption technologies. Since mass directly drives the cost of space systems, magnetic shielding can potentially make space exploration more affordable and hence more sustainable, a prime requirement of the new Space Exploration Vision. The concept of magnetic shielding is not new; the Earth has been doing it for billions of years! However, the ability to produce strong enough magnetic fields to enable magnetic shielding around spacecraft requires superconducting magnet technology that is only just becoming available. Many of the technical developments in space-qualified superconducting magnets referred to in this study were made as part of the AMS experiment currently scheduled to spend several years attached to the International Space Station. However, as revolutionary as these developments have been to date, they will not yet permit the construction of a sufficiently strong, large-volume, long-lasting magnetic field suitable for long-duration human space flight. We have studied the details of surrounding habitable volumes in human interplanetary spacecraft with a large magnetic shield. Using successively more accurate magnetic field models, we have shown that magnetic fields which are near the upper limit of current technological capabilities can indeed provide significant radiation shielding beyond the limits of what is expected from reasonable passive shielding configurations. If our research proceeds to Phase II, we plan to extend the shielding studies to even more accurate 3-dimensional magnetic shielding models. We also plan to examine other potential uses of superconducting magnet technology for human spaceflight.

Table of Contents

Abstract	1
Table of Contents	2
1. The Risk from Radiation	3
1.1 Types of Radiation	4
1.2 High-Energy Cosmic Rays – The effect of leakage through the radiation shield	4
1.3 Basic Principles of Magnetic Shielding	6
2. Preliminary study of magnetic shield for space radiation	8
2.1 Magnetic shield design	8
2.2 Simulation methods	9
2.3 Results	9
2.4 Discussion of results	16
3. Accurate grid calculation of magnetic field configuration for in-space shielding of humans from high-energy cosmic rays	17
3.1 Purpose of study	17
3.2 Magnetic shielding fundamentals	18
3.3 Detailed magnetic field calculations	19
3.3.1. Solving magneto-static equation in 2D on unstructured meshes	20
3.3.2. Direct calculation of magnetic field by current summation ..	21
3.3.3. Numerical algorithm for ΔB calculation in 3D	23
3.3.4. Coil decomposition into linear segments	24
3.3.5. Calculation of magnetic field for a system of toroidal coils ..	25
3.4 Analytical relativistic 3D3V orbit integrator for the $E=0$ case	26
3.5 Monte-Carlo calculations of radiation flux reduction	29
3.6 Discussion of results	32
4. Design considerations for a real superconducting magnetic shield system	32
5. Summary of calculations and further directions for research	34
6. Media Interest and Outreach	35
6.1 External interest in this research	35
6.2 Presentation to the Physics community	37
References	38

1. The Risk from Radiation

1.1 Types of Radiation

Solar Particle Events

Outside the Earth's trapped radiation belts, two fundamental sources of radiation threaten the health of space travelers: solar particle events (SPEs) and galactic cosmic radiation (GCR). Solar Particle Events consist mostly of low to moderate energy protons thrown into interplanetary space by coronal mass ejections. SPEs cannot currently be predicted in advance, but the frequency of SPEs is correlated with solar activity. Figure 1.1 shows typical spectra of strong SPEs. The danger to astronauts from SPEs is statistical, both because SPEs are relatively infrequent and because any given SPE will only affect spacecraft located in the zone of the solar-interplanetary magnetic field lines along which SPE charged particles are constrained to travel. Nevertheless, strong SPEs can deliver potentially lethal acute doses of radiation to unprotected astronauts. As an example, 5 Sv is generally recognized as a lethal dose, and the August 1972 SPE would have exposed Apollo astronauts to an estimated 10 Sv [Letaw, et al., 1987]. However, since SPE proton energies are almost all <1 GeV, they can be shielded against either with passive shielding or by the proposed magnetic shielding system.

Galactic Cosmic Radiation

Galactic cosmic radiation, consisting mostly of protons, alpha particles, and nuclei of heavier elements, is isotropic and pervades the solar system. Lower energy GCR can be scattered by irregularities in the solar-interplanetary magnetic field, which propagate outwards from the sun with the solar wind. Because such irregularities are correlated with solar activity, the intensity of low-energy GCR is anti-correlated with the solar activity cycle. The effects of scattering decrease at higher GCR energies, so the degree of variation with the solar activity cycle decreases at increasing energies. (Actually the deflection by magnetic fields is a combined function of the momentum and charge of a particle. For a given fully ionized element, "rigidity" increases with energy.) Figure 1.1 also shows the GCR proton spectrum at solar minimum and solar maximum.

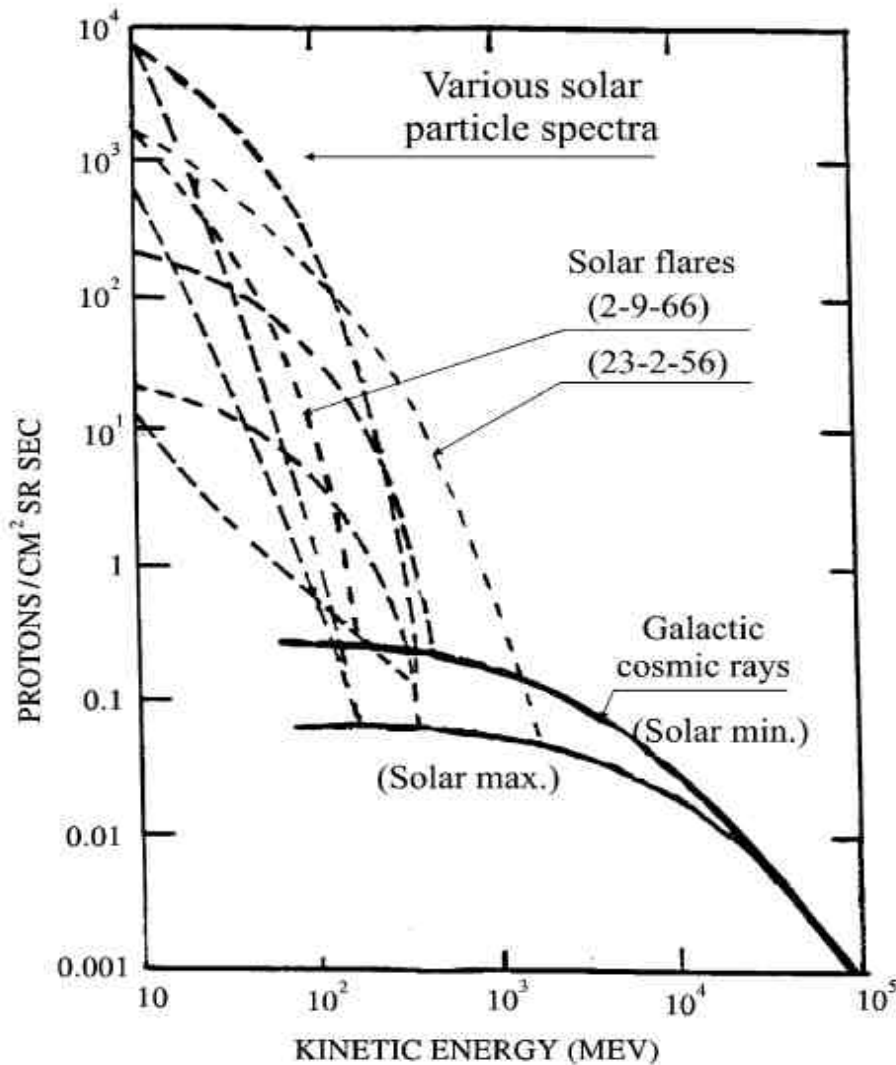


Figure 1.1 – Solar and cosmic proton energy spectra [Spillantini, et al., 2000]

1.2 High-Energy Cosmic Rays – The effect of leakage through the radiation shield

Any type of radiation shielding has an upper limit to the energy of particles against which it can shield. Above this energy, there will be leakage through the shield. However, the effects of this leakage differ greatly between magnetic shielding and passive absorption shielding. Spacecraft structures have traditionally been made of aluminum, and many studies and measurements have been done to show cosmic ray shielding by different thicknesses of aluminum. Results are shown in Fig. 1.2.

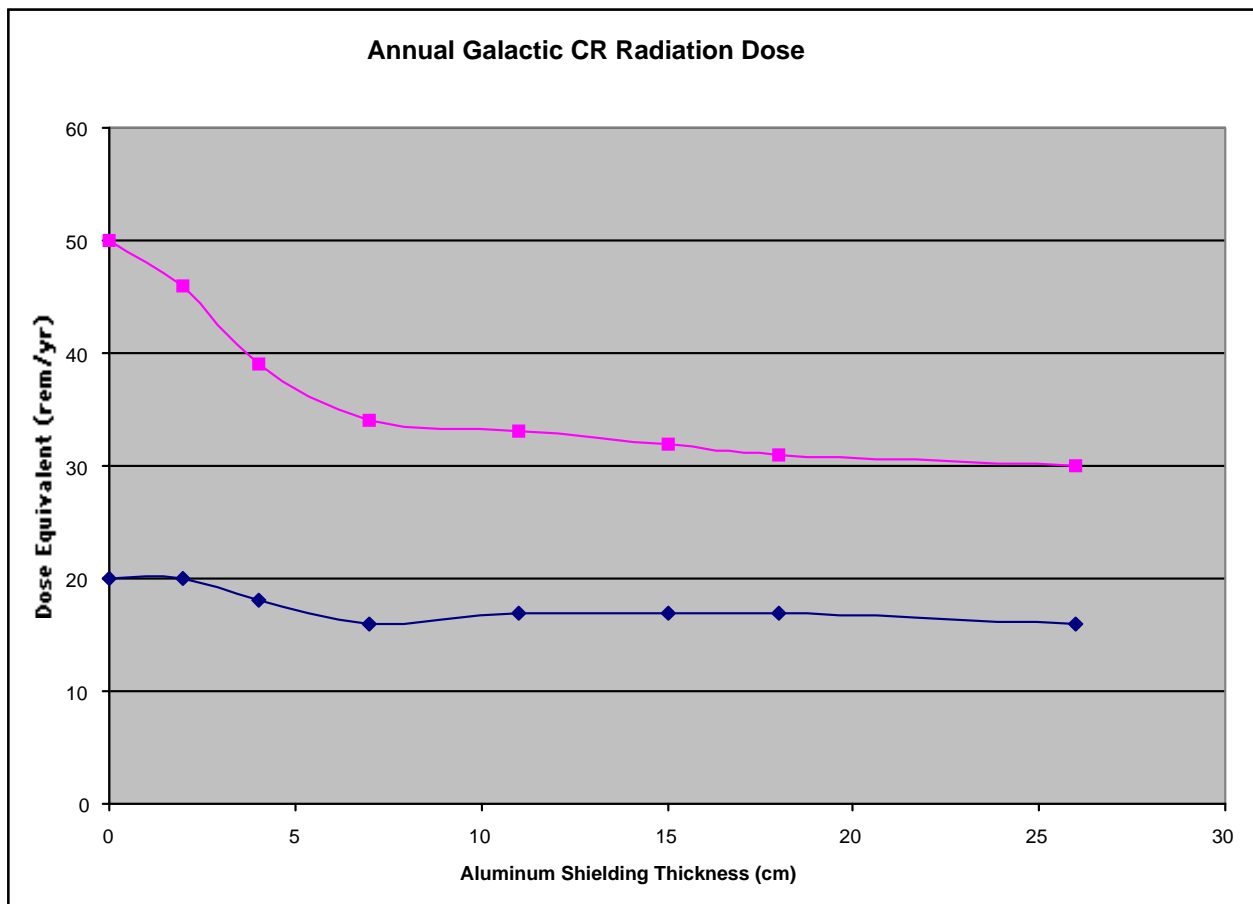


Figure 1.2 – Radiation doses received from galactic cosmic radiation with difference thicknesses of passive aluminum shielding. (Top curve: solar minimum; Bottom curve: solar maximum)

Passive shielding can be quite effective for particles with energies < 1 GeV/nucleon. However, for higher energy particles, nuclear interactions with the shielding material produce secondary particles which can actually be more numerous and detrimental to astronaut health than the incident radiation. Figure 1.2 shows that the first ~10 cm. of aluminum partially reduces the radiation, but doubling the thickness produces almost no more net reduction. If the thickness is increased sufficiently, of course, all radiation can be absorbed, but the resulting mass will be impractically large.

The magnetic shield described in this report will bend away cosmic ray protons with kinetic energies below ~2 GeV, depending on field strength and geometry. (Optimizing the limit through an investigation of the scaling characteristics of the superconducting magnet systems is one of the primary research areas for this study.) Although cosmic rays above some critical energy will certainly penetrate the shield, they pose a smaller danger, since although they have higher kinetic energy, they lose energy at a lower rate than lower energy cosmic rays. Above a kinetic energy of 4 GeV/nucleon, cosmic rays lose energy at a constant linear rate; so, for example, an alpha particle (charge 2) will lose ~120 MeV passing through a human body whether its total energy is 10 or 100 GeV/nucleon. Below about 1 GeV/nucleon, however, cosmic ray energy loss goes like $1/v^2$; so an alpha particle with 500 MeV/nucleon will deposit *all* of its energy in the human body, a total of 2 GeV, or sixteen times as much as a 10-100 GeV/nucleon alpha. This is one reason why the 2-4 GeV/nucleon energy range is critical for our study.

Passive shielding only makes the problem worse for high-energy cosmic rays, which interact in the shielding to create secondary particles with a higher “quality factor” (i.e. more physiologically damaging) than the primary radiation. Using hydrogen as a passive shield reduces but does not eliminate secondary shower generation. This fundamental difference between magnetic and passive shielding is inherent in the physics of particle interactions. It represents a fundamental advantage of magnetic shielding over and above the potential reduction in shielding mass. In other words, higher energy cosmic rays which penetrate the magnetic shield will do less damage than the secondary particles emerging from the interaction of those same higher energy cosmic rays with passive, absorption shielding.

The Principal Investigator for this study acknowledges useful conversations with Dr. Frank Cucinotta of the Johnson Space Center’s radiation protection group. Dr. Cucinotta [private communication] explained the tremendous complexity in translating radiation spectra into actual physiological dosages. Following his advise, we concentrated our efforts on predicting the modification of the radiation spectrum penetrating the magnetic shield rather than attempting precise dosage conversions on our own. Dr. Cucinotta’s group can take our spectra and use their specialized modeling software to transform these spectra into actual dosages. Dr. Cucinotta believes that a reasonable mass of passive shielding can protect astronauts up to energies of ~ 1 GeV/nucleon. The critical energy range is ~ 2 -4 GeV, where the effectiveness of both passive and magnetic shielding falls off rapidly. The results we present in the following sections will concentrate on examining the reduction in radiation in this critical energy range.

1.3 Basic Principles of Magnetic Shielding

Magnetic shielding has been the subject of several previous studies [Landis, 1991; Townsend, 2000]. We are studying this complex engineering problem on the basis of recent advances in technology and computational models. The following key points have to be taken into consideration for the theoretical studies and engineering design of a shielding system to protect astronauts from the cosmic rays:

- Charged particles can be either absorbed in a relatively uncontrolled way by various materials or actively reflected by stationary electric and/or magnetic fields.
- During the process of absorption, the composition and spectrum of the radiation changes. If absorption is not complete, the transformed radiation enters the habitable zone with effects potentially much worse than the original incident radiation. Secondary particles which were not present in the incoming radiation (e.g. neutrons) can be produced in the shielding material and enter the habitable zone.
- Reflection does not change the composition of the radiation; no new particles are created. Magnetic and electrostatic reflections have somewhat different effects on the incoming particle spectrum. In both cases, reflection has more of an effect on lower energy particles, so it effectively hardens the spectrum of radiation entering the habitable zone. A magnetic field does no work on charged particles, so it does not

change the energy of the incoming particles; it just diverts them. Thus, at all energies, the radiation penetrating the habitable zone is never greater than the incident radiation. Electrostatic deceleration actually lowers the energy of incoming particles, so the overall effect on the spectrum is more complex, as incoming particles at high relativistic energies are characterized not only by different masses, but also ionization states and velocity vectors at the impact.

No system can be purely reflective, since the mass of the reflecting system will interact with incoming particles. This is equivalent to partial shielding, which, as was stated above, can in some circumstances have deleterious effects.

We now present the results of two studies of the effectiveness of magnetic shielding. The first, presented in section 2 (carried out primarily by Peter Fisher) uses simplified magnetic field models in order to give early indications of the performance of the system. The second, presented in section 3 (carried out primarily by Oleg Batishchev) uses a much more accurate calculation of the magnetic field for a given coil geometry. This work is still in progress. We present the current state of the results in order to show that there are some differences from the simplified field model calculations presented in section 2. We will continue to develop the more accurate field models in a full 3-dimensional calculation if this research progresses to Phase II.

2. Preliminary study of magnetic shield for space radiation

(done primarily by Peter Fisher)

Our initial study of the reduction in radiation exposure inside a magnetically shielded habitable volume assumed the conceptual design geometry as shown in Figure 2.1. The coils are assembled in a double-toroidal-solenoid configuration to repel particles coming from all directions and to create a sufficiently large inner habitat with vanishing magnetic field. (Note that although the indicated field magnetic strength in the figure is 5T, we actually did our initial calculations at higher fields, ~9T.)

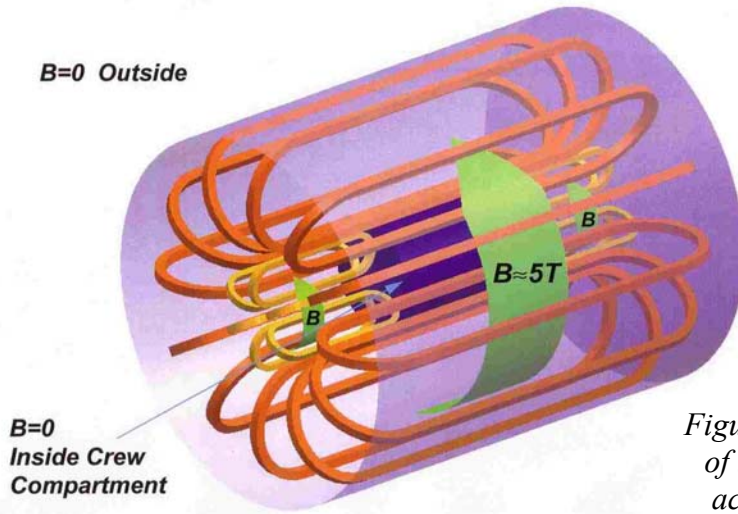


Figure 2.1 – Proposed assembly of the magnetic coils forming active shield around habitat

2.1 Magnetic shield design

The magnetic shield works by deflecting the incident charged particle radiation in a magnetic field. For a field \vec{B} , a particle of charge q moving with velocity \vec{v} will be subject to the Lorentz force $\vec{F} = q(\vec{v} \times \vec{B})/c = qvB \sin \theta / c$ where θ is the angle between the particle's velocity and the magnetic field. The Lorentz force always acts perpendicularly to the particle's direction of motion, causing the particle to travel along a curve. In the special case of a relativistic particle with Lorentz factor γ moving perpendicularly to a magnetic field, the trajectory will be circular with radius $\rho = m\gamma v / \kappa B$ where $\kappa = 0.3 \text{ GeV/T} - \text{m}$.

The idea for magnetic shielding of a spacecraft relies on a toroidal magnetic field surrounding the habitable volume, Figure 2.1. Oval coils arranged circularly around the habitat create the field, which is oriented circularly around the axis of the habitat. Charged particles incident from outside the shield will then always have some component of their velocity perpendicular to the magnetic field and will thus be subject to the Lorentz force.

As a start, we chose a magnetic field of 9 T (which is 90,000 G), which has been achieved in large magnets for accelerators (the Large Hadron Collider at CERN). Studies indicate that the most damaging dosage in space comes from cosmic rays having energies below about 2-4 GeV/nucleon. Using the equation above, we find a field thickness of 1.5 to 3 meters is required for complete protection. NASA requirements for the dimensions of a habitat for an interplanetary flight are a diameter of 7 m and a height of 7 m (116 m³) for a cylindrical habitat. For our baseline study, using a field thickness of 1.5 m gives outer dimensions of 10 m diameter and 10 m height.

2.2 Simulation method

Our calculation is based on the Monte Carlo method: for each energy, we start particles just outside the outer surface of the shield with an isotropic velocity distribution. The particles start randomly just outside the surface of the shield. The trajectory is then calculated in approximately 0.5 cm steps using the Lorentz force law. We count the total number of particles which traverse the magnetic field and enter the habitat, using 100,000 trials for each energy. The simulation is carried out with and without a magnetic field for each energy and the energy ratio: $R = (\text{number entering no field})/(\text{number entering with field})$ gives the flux reduction factor. R approximates the dose reduction factor to about 20% and we treat them the same for the purposes of this preliminary study.

We have run several different calculations:

1. Baseline – 9 T uniform field with the dimensions given above
2. Uniform field of 9.2 T with the dimensions given above.
3. Uniform field of 9 T with a field thickness of 1.7 m.
4. A somewhat more “realistic” field with radial dependence of the form

$$\vec{B} = B_o(r_o/r)\hat{\phi} \text{ with } r_o \text{ chosen such that } \langle BL^2 \rangle = \int_{r_{in}}^{r_{out}} B(r)rdr = 20.25T - m^2.$$

This case has a 50 cm radius zero field region at each end to account for the inner coils in an approximate way.

This last case deserves some explanation: for a uniform field of thickness L , the bending is BL^2 . For the coil arrangement shown in Fig. 2.1, the field will have an approximate $1/r$ dependence, and we take the case where we increase the magnetic field in order to have the same bending power.

Once we have $R(E)$, we can compute the reduced flux inside the habitat. $\Phi_i = F_i E^{-2.7}$ gives the flux for elemental species i with kinetic energy E per nucleon. The values for F are given in Table 2.1. The flux inside the habitat is then just $\Phi_{i,inside}(E) = \Phi_i(E)/R(E)$.

2.3 Results

Figure 2.2 shows the flux reduction in protons for the baseline case. All protons below about 2 GeV are completely rejected and 50% of 3 GeV protons are rejected. The curves for heavier elements look similar with rejections somewhat lower owing the lower Z/A ratio. Table 2.1 gives the fractional contribution to the flux inside the habitat for each

element. Comparing the flux with and without the magnetic field, we find the total flux, which is approximately the total dose, is reduced by a factor of 10.7.

Turning next to the radially dependent, more “realistic” B-field case described above, Figure 2.2 also shows a comparison for the reduction factor between the “realistic” and ideal cases. Adding up the dose gives a reduction of 3.3. We note the “realistic” case underestimates the reduction factor, as it does not include the fringe fields from the coils. Also, the 50 cm hole will contain the coils and will most likely absorb all the particles entering.

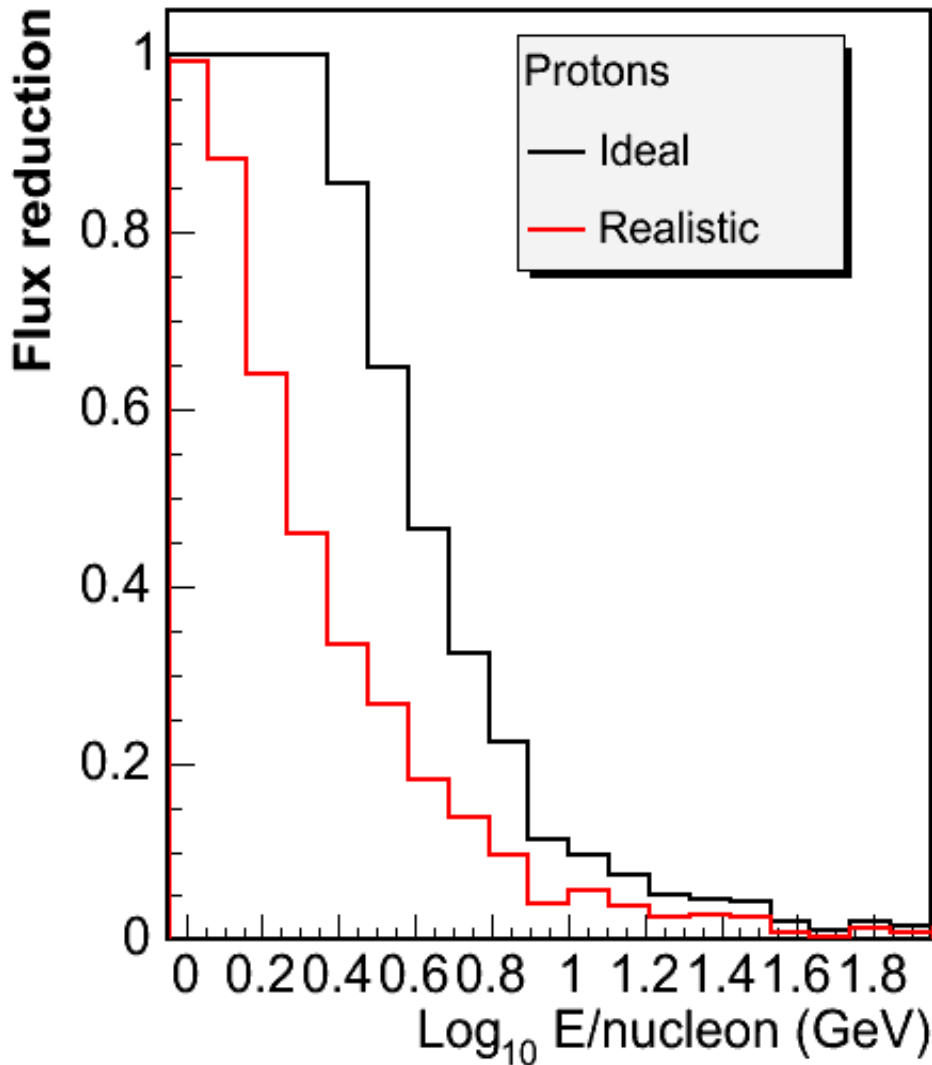


Figure 2.2 - Comparison of ideal case and realistic cases
(2-4 GeV corresponds to 0.3-0.5 on the logarithmic scale.)

Next, we consider some changes in the design parameters. Figure 2.3 shows the ideal and realistic cases with 9 T and 9.2 T fields; the reduction factor increases to 11.1 for the 9.2 T case, giving $dR/dB = 1.8/T$. A 20% change in the field results in a 20% improvement in flux reduction.

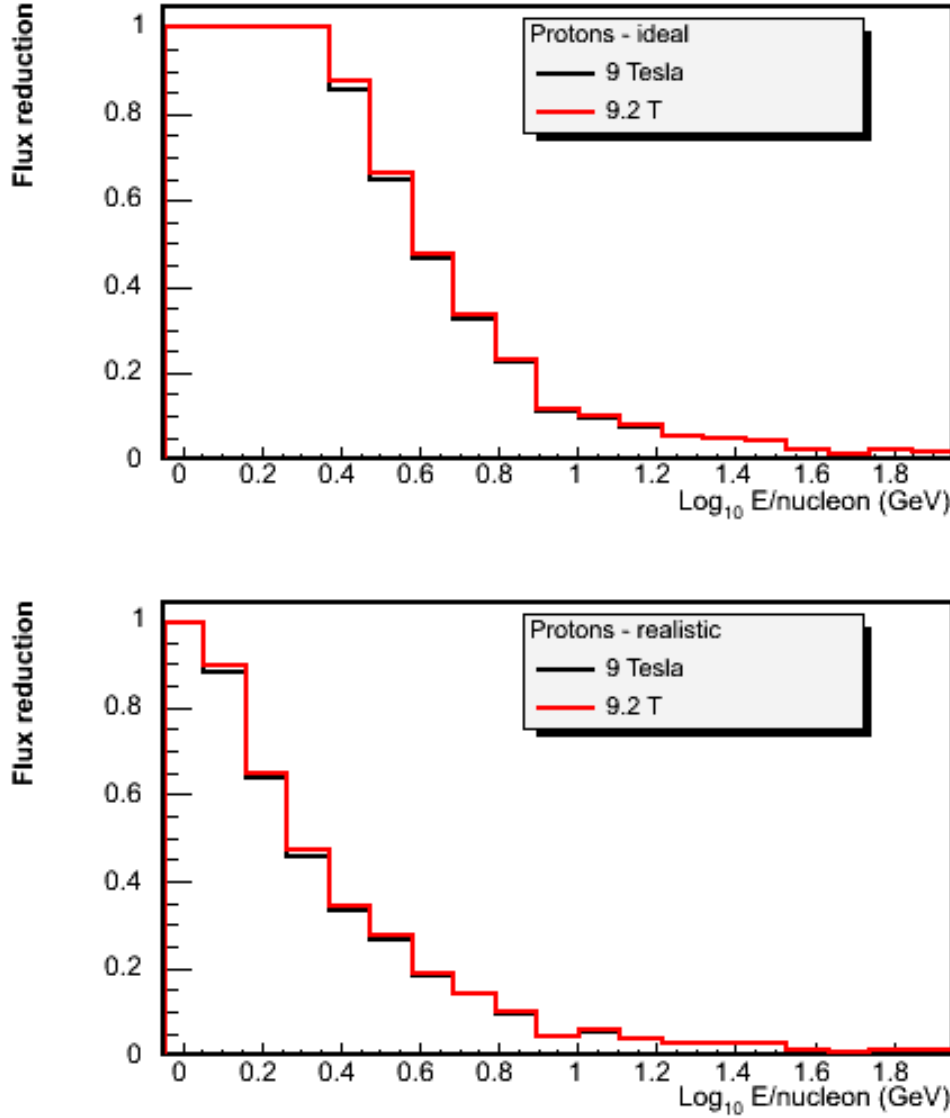


Figure 2.3 - Comparison of ideal and realistic cases with 9 T and 9.2 T fields.

Finally, the calculation of the dose was carried out for a $L=1.7$ m field thickness, resulting in a reduction factor of 13.1 (Fig. 2.4). This gives $dR/dL = 12/m$. Thus, a 20% change in field thickness gives a 30% change in reduction factor. These two results follow from the bending power being proportional to BL^2 ; for a given fractional increase, the bending power improves more if the field thickness increases than if the magnetic field increases.

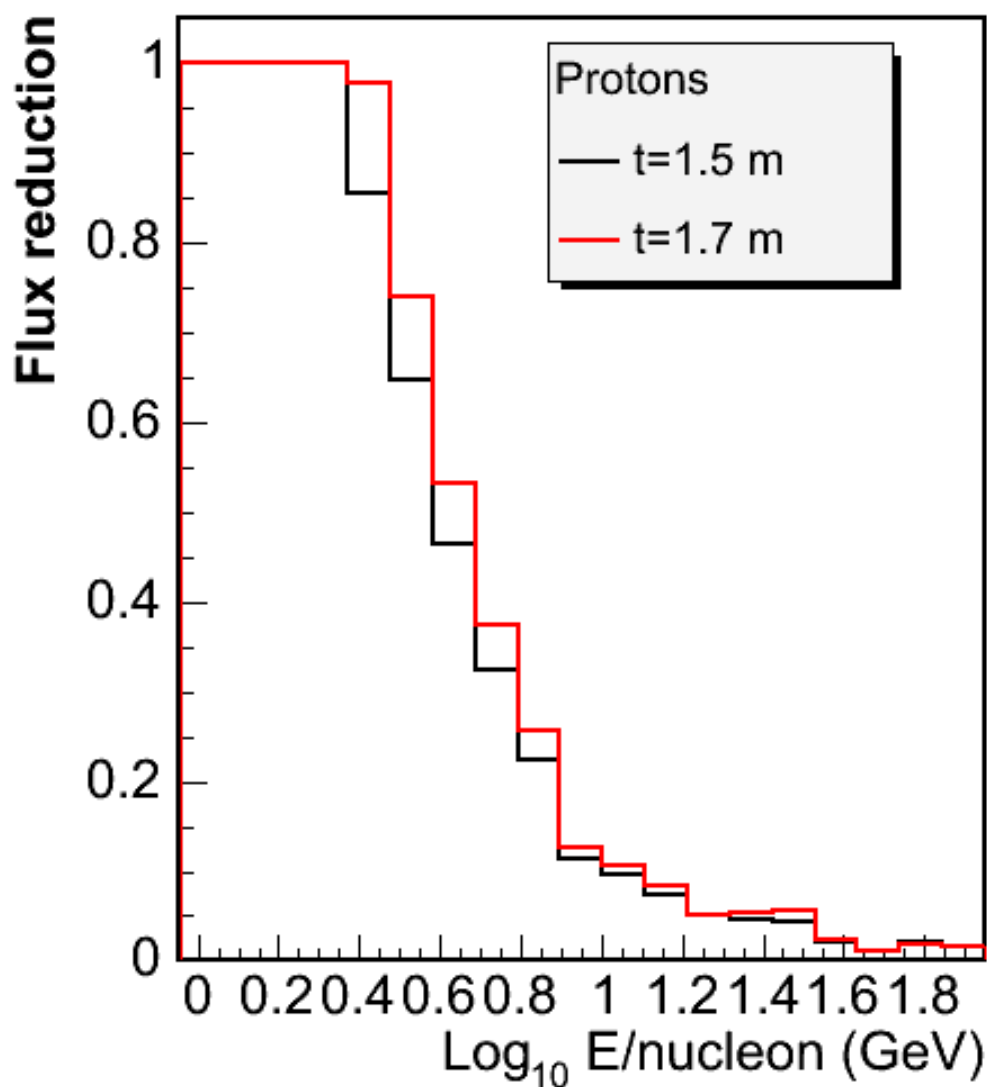


Figure 2.4 - Comparison for the ideal case with 1.5 m and 1.7 m thick magnetic field regions.

Figure 2.5 – 2.7 show comparisons of the flux with and without the magnetic field for all species of cosmic radiation from protons through $Z=27$ (cobalt). The transmitted spectra can be added, using the abundance factors given in Table 2.1, to give an overall dosage. The radiation in free space is ~ 90 rem/yr, with a total dose of 300 rem considered lethal. Our baseline design would reduce the dose to ~ 9 rem/yr, and the dose for a three-year mission would be below 10% of the lethal dose.

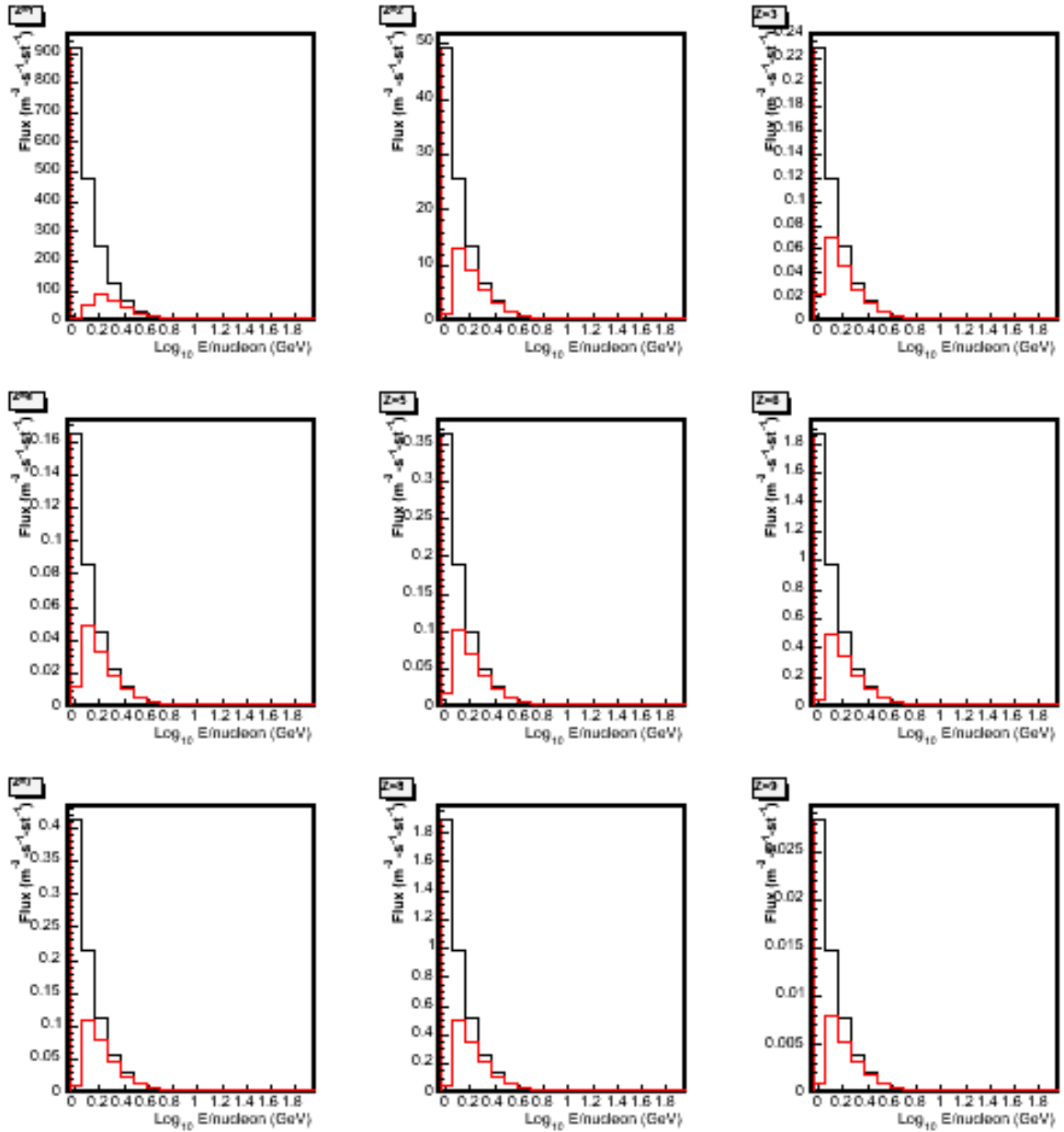


Figure 2.5 - Comparison of spectrum in the habitat with and without the ideal case magnetic field for elements $Z=1-9$.

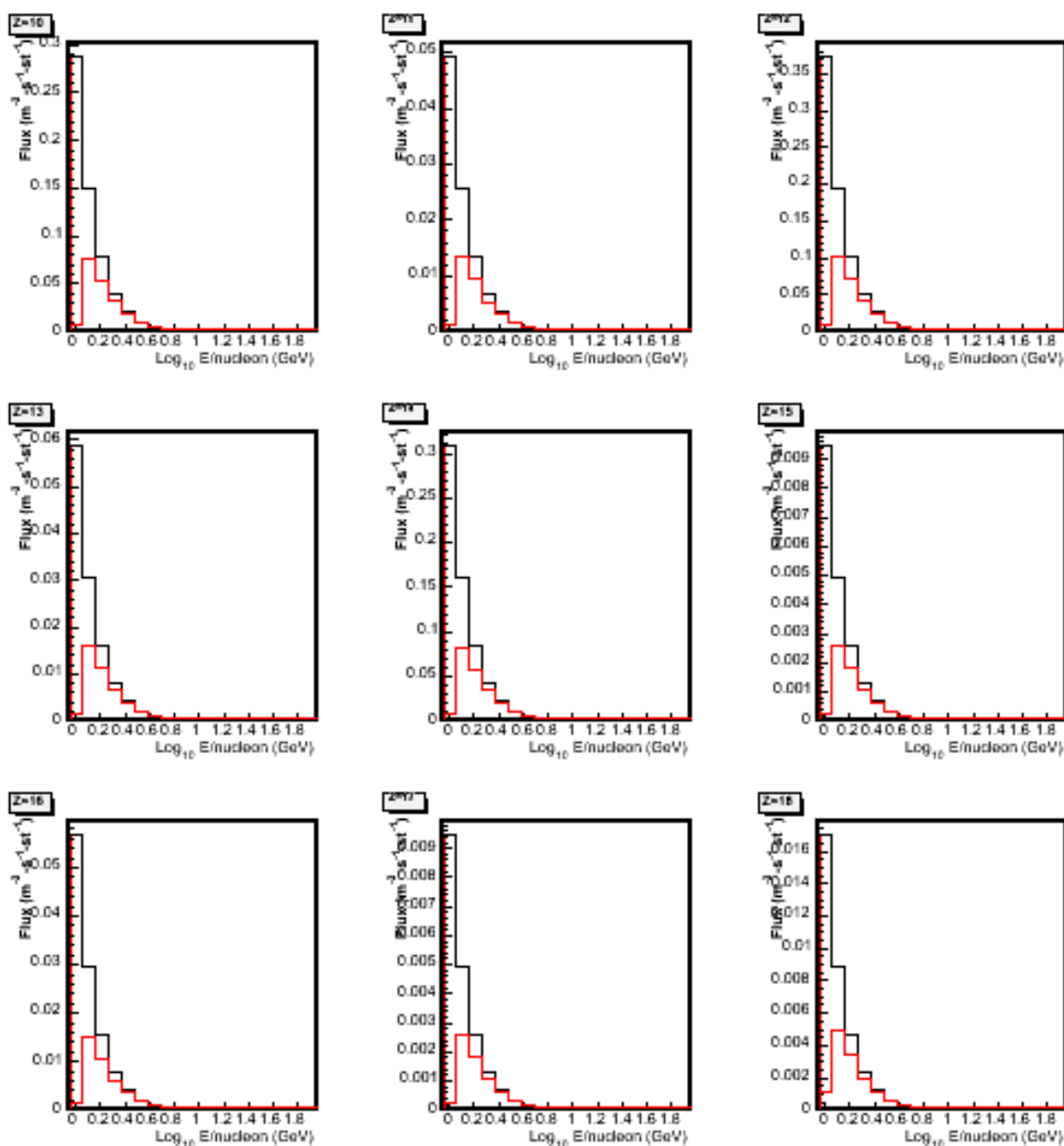


Figure 2.6 - Comparison of spectrum in the habitat with and without the ideal case magnetic field for elements $Z=10-18$.

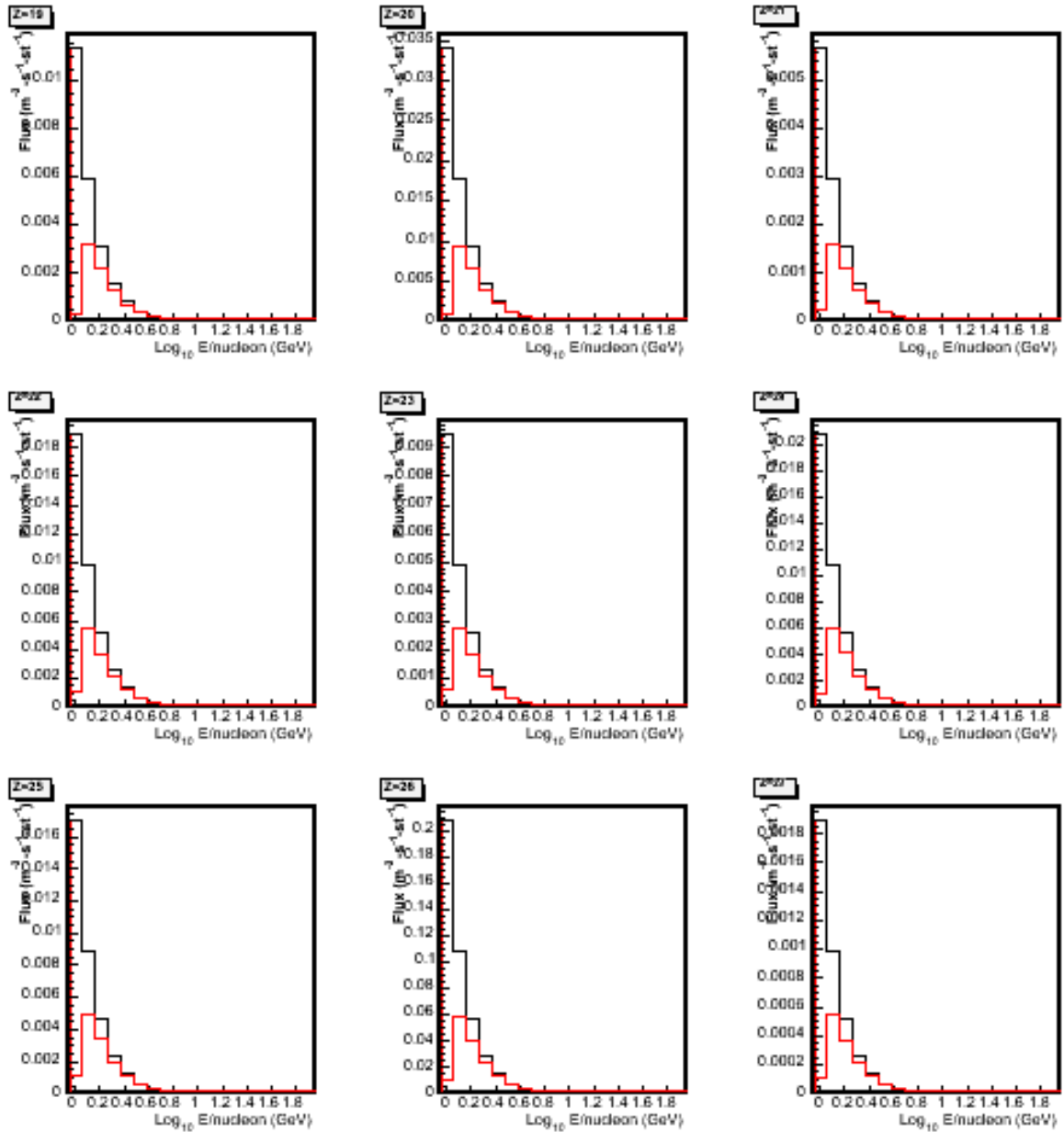


Figure 2.7 - Comparison of spectrum in the habitat with and without the ideal case magnetic field for elements $Z=19-27$.

Z	M	F	%dose	Z	M	F	%dose
1	1	485	0.12	15	31	0.005	0.19
2	4	26	0.30	16	32	0.03	1.4
3	7	0.121	0.0084	17	35.45	0.005	0.32
4	9	0.087	0.018	18	40	0.009	0.77
5	10.8	0.192	0.095	19	39	0.006	0.58
6	12	0.986	0.91	20	40	0.018	2.1
7	14	0.218	0.37	21	45	0.003	0.45
8	16	1	2.9	22	47.867	0.01	1.8
9	19	0.015	0.076	23	51	0.005	1.1
10	20	0.152	1.1	24	52	0.011	2.9
11	23	0.026	0.28	25	55	0.009	2.8
12	24.3	0.197	2.9	26	55.485	0.110	39.6
13	27	0.031	0.66	27	59	0.001	1.9
14	28	0.163	4.5	28	58.69	0.007	15.4

Table 2.1 - Abundance and contribution to dose inside habitat for ideal case for each element.

2.4 Discussion of results

The effectiveness of the magnetic shielding in the modeling shown above decreases rapidly as the particle energy increases from 2 to 4 GeV/nucleon. Moreover, the effectiveness of the “ideal” and “realistic” magnetic field configurations (Fig. 2.2) differ considerably all the way up to 10 GeV/nucleon. This critical dependence on the detailed geometry of the magnetic field led us to initiate a more accurate calculation of the magnetic field, carried out primarily by Oleg Batishchev and described in the next section.

(Note that this work was originally written up independently. While we have attempted to integrate it seamlessly into the overall report, time constraints have not allowed us to do this completely. As a result, there is some overlap in the initial problem description in this section with what has been given earlier. Hopefully this will not cause confusion.)

3. Accurate grid calculation of magnetic field configuration for in-space shielding of humans from high-energy cosmic rays
(done primarily by Oleg Batishchev)

3.1 Purpose of study

This work consisted of developing a detailed transfer model of cosmic radiation through a combined region containing matter and a strong magnetic field. The goal of this calculation is to model the radiation penetrating the habitable volume. (Physiological effects of the penetrating radiation must be considered separately and will be based on the comparison of the total dose calculations with existing NASA biomedical data and approved standard radiation requirements.)

The model will at first be used to optimize the magnetic field configuration around the habitable volume, with no special consideration being given to the mass of the system producing the magnetic field. Since this model will represent as accurate a depiction of the magnetic field as possible, it will form the basis for further engineering studies of the magnetic shielding system.

Detailed space systems engineering design work will eventually produce a believable mass model associated with the assumed magnetic field. Elements to be considered are:

- Magnet Cores
- Windings
- Liquid He
- Mechanical Support for Magnets
- Cooling System (by assumption the power, propulsion and radiator systems are located away from habitable volume.)

With the resulting mass distribution, new radiation transfer calculations will yield a more accurate particle spectrum penetrating the habitable volume for the given magnetic configuration. This will allow an iterative process in which the magnetic field distribution is altered to minimize the penetrating radiation.

The engineering analysis has to be able to calculate the changing mass distribution as the field configuration is re-optimized to minimize the penetrating radiation; but as the iterations proceed, it also has to predict more accurately the real mass associated with the magnetic shielding system. The systems necessary for field maintenance (power, radiators, etc.) are located far enough away from the habitable volume so as not to have been taken into account for the scattering calculations. They will, however, have to be taken into account for the total mass budget.

3.2 Magnetic shielding fundamentals

Charge particles in a strong magnetic field are magnetized and follow adiabatic trajectories under the Lorentz force, which are strictly normal to the velocity vector in the absence of other fields, e.g. electric field:

$$\frac{d\vec{p}}{dt} = q \frac{\vec{v} \times \vec{B}}{c} \quad (1)$$

Here momentum and velocity are linked through the equality $\vec{p} = m_0 \gamma \vec{v}$ with the relativistic factor defined as $\gamma = \sqrt{1 + \frac{p^2}{m_0^2 c^2}}$; c is the speed of light in vacuum, and m_0 is the particle's mass at rest. A gyro-frequency of a particle placed in a uniform magnetic field is given by $\omega_H = \frac{qB}{m_0 \gamma c}$, with the corresponding gyro-radius:

$$r_H = \frac{v}{\omega_H} = \frac{v m_0 \gamma c}{qB} = \frac{pc}{qB} \quad (2)$$

For the ultra-relativistic particles with high energies $E \gg E_0 \equiv m_0 c^2$ the product of momentum times speed of light becomes increasingly close to the actual energy,

$$pc = \sqrt{E^2 - m_0^2 c^4} \rightarrow E, \quad (3)$$

and, therefore, $r_H \rightarrow \frac{E}{qB}$. In the commonly used units – *GeV* for energy E , *Tesla* for magnetic field, and if we measure dimensionless charge in units of electron charge $q/e=n$, the Larmor radius in meters reads as $r_H(m) \approx 3.336 \frac{E(GeV)}{nB(T)}$.

Finally, we arrive at a simple estimate of the required “magnetic thickness” of a shield stretching from point A to B that will reflect back all (ultra-relativistic and not) particles with energies equal or smaller than E regardless of their charge number:

$$E(GeV) < 0.3 \int_A^B B(T) dl(m) = 0.3 < B > \Delta \quad (4)$$

where we integrate along line $A-B$, Δ is the width of the magnetic layer carrying mean magnetic induction $< B >$. Of course, particles which are not ultra-relativistic will require weaker magnetic insulation. However, quantitative calculations of required thickness have to take into account processes that can change the speed of particles (not just rotate the velocity vector) and the entire energy spectrum of the population. This has to be done numerically, as purely theoretical analysis is limited due to the complexity of the system.

We started with the conceptual design of the targeted magnetic shield as presented in Fig. 2.1. The coils are assembled in a double-toroidal-solenoid configuration to repel particles coming from all directions and to create a sufficiently large inner habitat with vanishing magnetic field.

By choosing $\langle B \rangle = 5 - 7 \text{ T}$ and coil width $\Delta = 1 - 2 \text{ m}$ we can estimate that the cosmic ray spectrum can be significantly reduced at energies up to $E < 1.5 - 4.2 \text{ GeV}$. These numbers imply a 70-90% reduction of the cosmic ray flux (see Fig. 1) within the habitat. To reduce penetrating flux to 1% of the nominal intensity one has to achieve magnetic thickness on the order of $\sim 30 \text{ Tm}$.

Next, we can estimate currents I in the coils and magnetic forces F acting on them. Let us select the target number of coils to be $K=16$, and the large radius of the torus $R \sim 4-5 \text{ m}$.

A mean field inside a toroidal solenoid of major radius R is given by the expression:

$$B = \frac{\mu_0 N I}{2\pi R} = 2 \times 10^{-7} \frac{K I (A)}{R(m)} \quad (5)$$

By substituting input parameters, we estimate that to achieve 30 Tm the required current has to be substantial, $I \approx 10 \text{ MA}$. The forces acting on coils could be estimated as follows. The magnetic force per unit length acting on two parallel currents I separated by distance Δ is given by formula:

$$F(Nm^{-1}) = \frac{\mu_0 I^2}{2\pi \Delta} = 2 \times 10^{-7} \frac{I^2 (A)}{\Delta(m)} \quad (6)$$

which gives a linear force estimate on the order of $F \sim 10^7 \text{ Nm}^{-1}$ for the selected extreme physical/geometrical parameters. Note that the force drops rapidly as $F \sim K^{-2}$, when the number of coils is increased.

Naturally, the analysis presented above is accurate only to within roughly an order of magnitude. Actual fields are non-uniform; they peak near the coils and drop in the inner spaces. Moreover, the field has the strongest gradients inside the superconducting coils themselves. Because of the quite complex geometry of the system, quantitative analytical calculations of the magnetic fields, not to mention net shielding effect, are impossible. Therefore, computational models addressing relevant issues are being presently developed.

3.3 Detailed magnetic field calculations

There are several viable ways of calculating stationary magnetic fields created by a fixed, prescribed current distribution $\vec{j}(\vec{r})$:

- i) solving the Poisson equation for the vector-potential: $\nabla^2 \vec{A} = \vec{j}$, $\vec{B} = \nabla \times \vec{A}$;

- ii) solving the set of Maxwell equations with zero initial EM-fields and currents, but $\frac{d\vec{j}(\vec{r})}{dt} \neq 0$ until the currents are matched, and a steady-state regime is achieved;
- iii) direct calculation of the static magnetic field by using the Biot-Savart Law.

The first method is known to produce the smoothest fields. But it requires a spatial mesh, which is true for the second method as well. If the mesh is structured or uniform, both methods achieve poor accuracy in the coil vicinity, where the gradients are the highest. The only possibility to overcome this problem is to use non-uniform meshes. In general it leads to the utilization of the so-called unstructured grids and corresponding methods, characterized with a high level of numerical complexity.

3.3.1 Solving the magneto-static equation in 2D on unstructured meshes

In this section, we present as an example an application of the unstructured, adaptive non-uniform mesh method (Batishchev, et. al., 1999; 2003) to the problem of magnetic field calculation. Presently the method is developed for 2 dimensions only. Extension of the method to 3D will be proposed for Phase II research, as it requires major method/software development. However, when developed, it will give an unprecedented level of computational accuracy and flexibility from the geometrical standpoint.

The following Fig. 3.1 represents currents in 4 coils, mimicking 2D cross-section of the toroidal system shown in Fig. 2.1. All the dimensions are given in meters, while the equivalent current is set to 10 MA

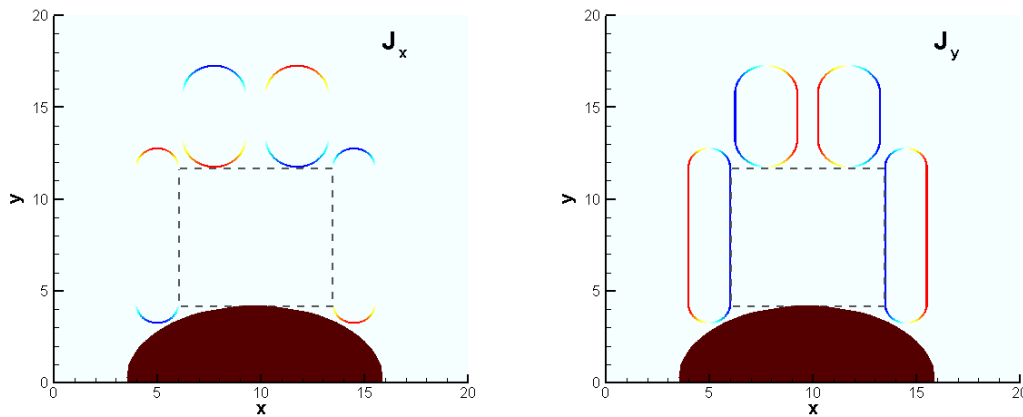


Figure 3.1 – Contours of the x- and y- components of currents in the superconducting coils

The magnetic field is strictly solenoidal in 2D, as $\frac{d}{dz} \equiv 0$ making coil currents equivalent to current sheets. Indeed, the calculated magnetic fields happen to be uniform within each of the coils, as could be seen from the following Fig. 3.2.

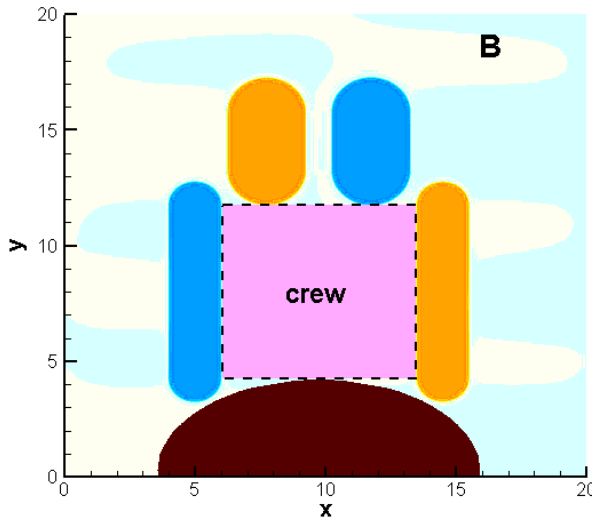


Figure 3.2 – Contours of the calculated magnetic field created by a system of 4 coils. Dark region at the bottom resembles space craft, to which the habitat is attached.

In the calculations presented here, we have assumed that coils have finite widths on the order of several centimeters. Therefore, the computational grid is finer in the coil vicinity, as automatically enforced by the preset accuracy condition. As an illustration, a particular section of the simulation domain was magnified and is presented in Fig. 3.3 below. One can see that the computational grid conforms to current density.

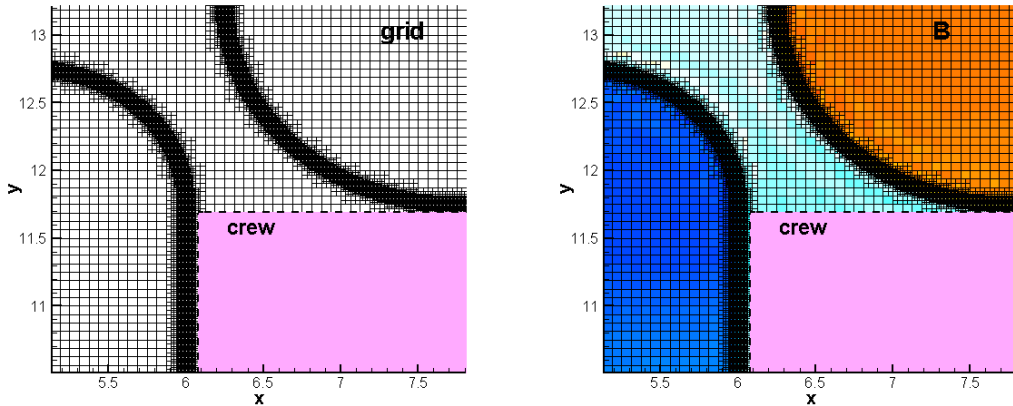


Figure 3.3 – Zoomed portion of the domain showing non-uniform grid conformed to j

With the adaptive 3D grid modeling being still under consideration for the future, we are left with the only option - direct magnetic field summation through the Biot-Savart Law. The corresponding procedure is described in the next sub-section.

3.3.2 Direct calculation of magnetic field by current summation

To calculate particle trajectories with this technique, a spatial mesh is not required, unless some Eulerian quantities have to be evaluated in the entire space, e.g. densities of the species, radiation fluxes, etc. However, direct summation is a computationally demanding

task, as it requires multiple summations over elementary currents. For this reason, we presently are calculating 3D magnetic fields on a structured cubic grid. Note that the very similar procedure could be (and will be) applied in case of the 3D adaptive mesh approach, which is more accurate, but has not yet been developed.

In the direct summation method arbitrarily distributed current is decomposed into a big number of thin linear segments. To each of these straight $\vec{l} = \int d\vec{l}$ segments we apply the Biot-Savart law:

$$\Delta \vec{B}_i(\vec{r}) = \int_i d\vec{B} = \int_i \frac{\mu_0}{4\pi} I \frac{d\vec{l} \times \vec{r}}{r^3} \quad (7)$$

This integral is easily evaluated as shown in planar Fig. 3.4. The magnetic field is normal to the current-radius-vector plane, so the vector product in the numerator reduces to a product $dl r \sin \theta$, where d is a distance from the line (AB) to point S , located at radius-vector \vec{r}_s . By using the geometrical relations $l = -d \cot \theta$ and $d = r \sin \theta$, the integral contribution (5) from the i -th segment could be calculated as:

$$\Delta \vec{B}_i(\vec{r}_s) = \frac{\mu_0}{4\pi} I_i \frac{\cos \theta_A - \cos \theta_B}{d} \vec{b}_i, \quad (8)$$

where \vec{b}_i is a unit vector in direction of magnetic field increment $\Delta \vec{B}_i$.

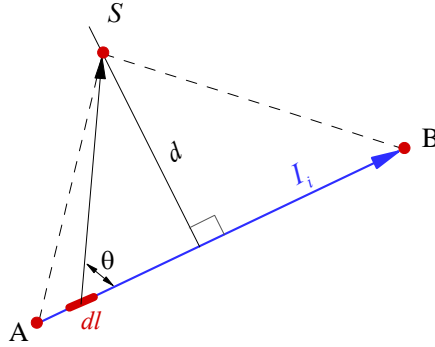


Figure 3.4 – Schematics of the calculation of an integral contribution to the magnetic field from a segment $[AB]$.

Expression (6) has to be evaluated for every spatial grid node s with respect to every current segment $i=1, \dots, M$ to obtain a local value of magnetic field:

$$\vec{B}(\vec{r}_s) = \sum_{i=1}^M \Delta \vec{B}_i(\vec{r}_s) \quad (9)$$

If the number of nodes is K , $s=1, \dots, K$, the total number of operations (9) is proportional to $K \times M$. The product could be large, but in any case, calculation of a static magnetic field has to be performed just once for a given configuration of the coils.

The details of actual computer realization of this approach are a bit more complicated. For instance, all coordinates are 3-dimensional, not 2 as shown in Fig. 3.4. The actual plane, holding all three points - S , A , B , as well as the normal distance d and cosines, has to be determined for each of the KM grid point – current segment pairs.

3.3.3 Numerical algorithm for ΔB calculation in 3D

To calculate ΔB one has to evaluate all terms in expression (8). The easiest way is to use vector algebra. Fig. 3.5 serves as illustration to the numerical procedure.

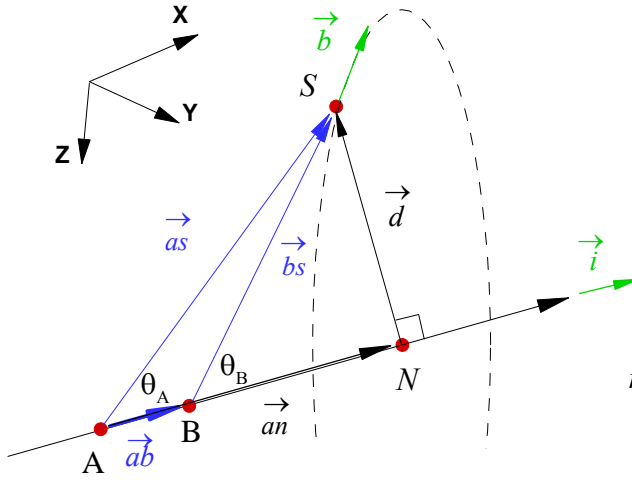


Figure 3.5 – Chart to illustrate numerical procedure for calculating magnetic field at point S created by segment $[AB]$

What is known – coordinates of 3 key points: A , B and S , defined by radius vectors \vec{r}_a , \vec{r}_b and \vec{r}_s , respectively. The rest has to be derived in an efficient way.

The first step is calculating vectors $\vec{ab} = \vec{r}_b - \vec{r}_a$, $\vec{as} = \vec{r}_s - \vec{r}_a$ and $\vec{bs} = \vec{r}_s - \vec{r}_b$.

Second step is finding cosines of angles θ_A and θ_B (Fig. 7) through scalar product, e.g.

$\vec{as} \bullet \vec{ab} = (x_s - x_a)(x_b - x_a) + (y_s - y_a)(y_b - y_a) + (z_s - z_a)(z_b - z_a)$, as:

$$\cos \theta_A = \frac{\vec{as} \bullet \vec{ab}}{|\vec{as}| |\vec{ab}|}, \quad \cos \theta_B = \frac{\vec{bs} \bullet \vec{ab}}{|\vec{bs}| |\vec{ab}|} \quad (10)$$

where the denominator uses the vector modulus, e.g. $|\vec{ab}| = \sqrt{\vec{ab} \bullet \vec{ab}}$.

Next we can find coordinates of point N , the start of segment NS , normal to line (AB) .

$$\vec{an} = |\vec{an}| \vec{i} = |\vec{as}| \cos \theta_A \frac{\vec{ab}}{|\vec{ab}|} \quad (11)$$

where \vec{i} is a unit vector in the direction of current.

Now one can obtain required distance d (see Figs. 3.4 and 3.5) as:

$$d = |\vec{d}| = \left| \vec{as} - \vec{an} \right| \quad (12)$$

The last step is using the now-known vectors \vec{i} and \vec{d} to construct unit vector \vec{b} , pointing in the direction of magnetic quanta $\Delta\vec{B}$. To find it, a vector product is used:

$$\vec{B} = \vec{d} \times \vec{ab} \quad , \quad \vec{b} = \frac{\vec{B}}{|\vec{B}|} \quad (13)$$

Final result is obtained combining operations (10) through (13) together.

3.3.4 Single coil decomposition into linear segments

For magnetic field calculations we use the following standard units: meter for length, Ampere for currents, and Tesla for magnetic field strength.

We assume that a single superconducting coil has a simple configuration as shown in Fig. 3.6a. As follows from this figure, the coil is basically a combination of two half-circular pieces of the same radius R , connected together with two straight segments of length L to form a loop. The same constant current I passes through every cross-section of the coil, which is assumed to be fixed as well, see Fig. 3.6b.

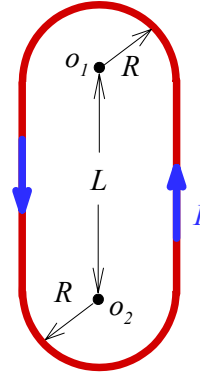


Figure 3.6a – Geometry of a coil used in analysis

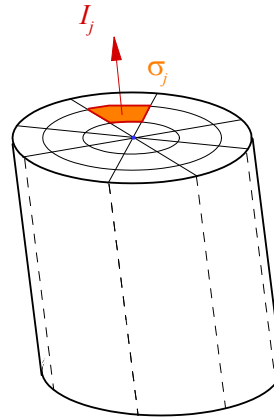
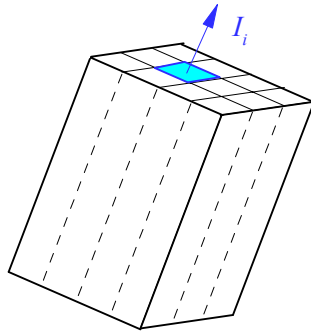


Figure 3.6b – Scheme of the coil currents decomposition into segments with sufficiently small cross-sections σ_j and currents I_j , depending on the shape of the coil.

The decomposition of superconducting coil currents into the straight current segments depends on the shape of the coils and on the desired accuracy. Two standard examples of subdivision of two linear currents with rectangular and circular cross-sections are presented in Fig. 3.6b. Partial static current I_j is calculated as directly proportional to the cross-section σ_j of this segment. Curved stretches of the magnetic coil are approximated by dividing them into a finite number of linear segments.

3.3.5 Calculation of the magnetic field for a system of toroidal coils

The proposed assembly of magnetic coils, presented in Fig. 2.1, is a combination of sub-coils with toroidal geometry. The larger coil assembly creates a sidelong shield. Due to the azimuthal symmetry a several meter-sized habitat cannot be protected against the radiation coming axially, and secondary shielding is required. One of the possibilities is to use a magnetic plug with a toroidal shape as well.

For magnetic field calculations we again use the following dimensional units: meter for length, Ampere for currents, and Tesla for magnetic field strength.

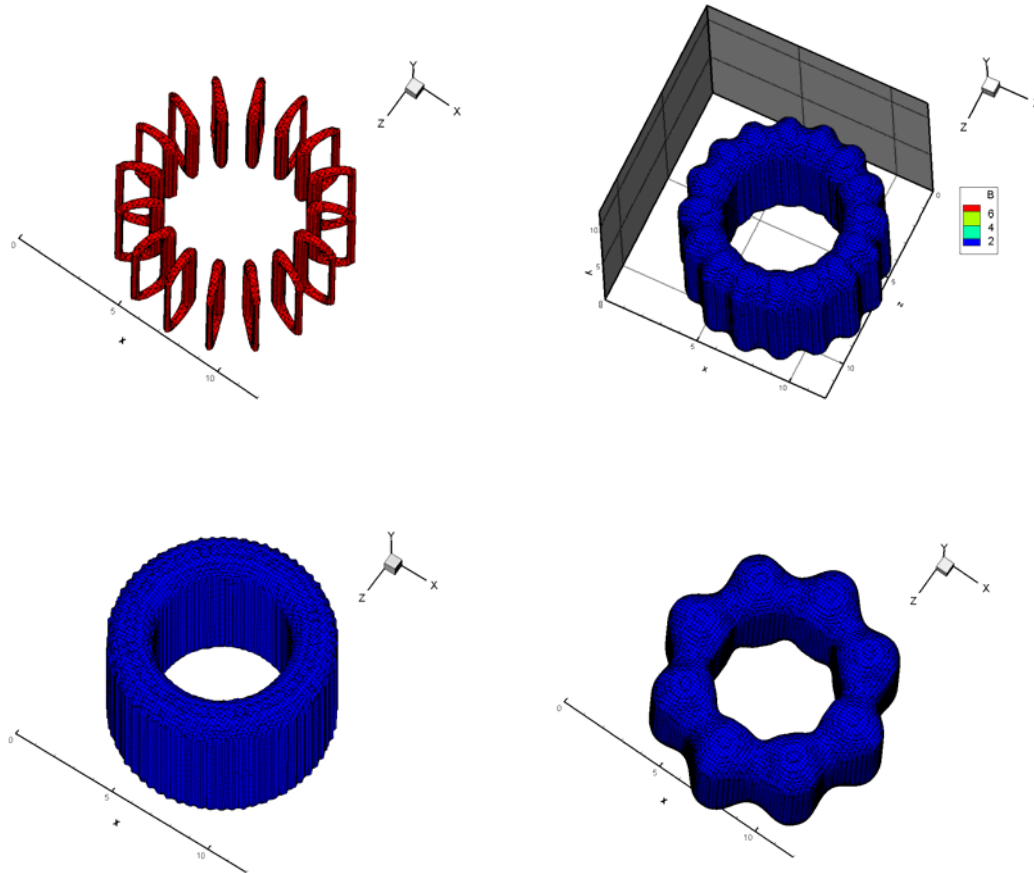


Figure 3.7 – Top: K=16 magnetic coil assembly, and corresponding magnetic field; for comparison a magnetic field for K=64 and K=8 is shown at the bottom with the coil currents accordingly scaled.

The numerical code can combine several toroidal configurations, as shown in Fig. 3.7. For instance, it can calculate the B-field distribution for the coil assembly shown in Fig. 2.1. An example of a system with 16-coil main magnet and a 8-coil magnetic plug is presented in Fig. 3.8.

After the magnetic fields are obtained we can integrate particle trajectories in these fields to calculate radiation flux distribution inside the system. There are several approaches to the orbit integration. We have developed the following analytical method, which is accurate and stable.

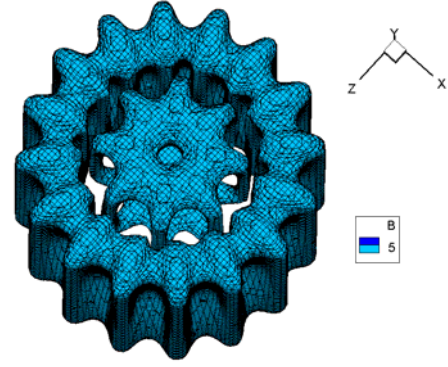


Figure 3.8 – Magnetic field of a system with $K=16$ coils and a $K=8$ magnetic plug at one end.

3.4 Analytical relativistic 3D3V orbit integrator for the $E=0$ case

In the general 3D3V relativistic case, the trajectory of any macro-particle (omitting species index) reads in the natural units as:

$$\begin{cases} \frac{d\vec{r}}{dt} = \vec{v} = \frac{c \vec{p}}{\sqrt{m_0^2 c^2 + p^2}} \\ \frac{d\vec{p}}{dt} = q \left(\vec{E} + \frac{\vec{v} \times \vec{B}}{c} \right) \end{cases}, \quad (14)$$

$\vec{p} = m_0 \gamma \vec{v}$ is the relativistic momentum $\vec{p} = m_0 \gamma \vec{v}$, where m_0 is the mass at rest, and the square of the relativistic factor $\gamma^2 = \frac{c^2}{c^2 - v^2} = 1 + \frac{p^2}{m_0^2 c^2}$.

We are using semi-analytical procedure to integrate (14), which unlike a traditional finite-difference approach, guarantees that the particle will stay on a correct helical orbit for an arbitrary number of time steps. Importantly, the analytical algorithm is unconditionally stable, conservative, accurate, and has correct asymptotics.

In the case of a vanishing electric field Eq. (14) can be integrated analytically in the relativistic case of interest. First, the second equation reduces to:

$$\frac{d\vec{p}}{dt} = q \frac{\vec{v} \times \vec{B}}{c} \quad (15)$$

By calculating a scalar product by \vec{v} , one proves that the amplitude of momentum (and velocity) does not change in time:

$$\vec{v} \cdot \frac{d\vec{p}}{dt} = \frac{1}{2m_0 \gamma(\vec{v})} \frac{dp^2}{dt} = q \vec{v} \cdot \frac{\vec{v} \times \vec{B}}{c} = 0 \quad (16)$$

Basically, this means that the trajectory of a particle can be viewed as classical with scaled mass $m = m_0 \gamma$. The problem could be formulated as follows: from the known phase coordinates of a particle $\{\vec{r}_1, \vec{v}_1\}$ at the time t calculate new coordinates $\{\vec{r}_2, \vec{v}_2\}$ at the next time moment $t + \Delta t$ assuming that the magnetic field is fixed.

To simplify orbit integration, we split the particle's 3D3V trajectory into two independent motions – along the direction of the magnetic field, and in the plane normal to \vec{B} . The following sketch illustrates the corresponding numerical procedure.

The parallel and perpendicular projections of the initial velocity \vec{v}_1 with respect to the direction of the field vector \vec{B} are obtained using the scalar product:

$$\begin{cases} \vec{v}_1^b = (\vec{v}_1 \vec{b}) \vec{b} = v_1^b \vec{b} \\ \vec{v}_1^n = \vec{v} - v_1^b \vec{b} = v_1^n \vec{n} \end{cases}, \quad (17)$$

where $\vec{b} \equiv \vec{B} / B$ is a unit vector in the direction of the magnetic field. Another unit vector $\vec{n} = \vec{v}_1^n / v_1^n$ is normal to \vec{b} . These two vectors, along with a third unit vector (a vector-product, of the two, $\vec{u} = \vec{b} \times \vec{n}$) form a right-handed coordinate system shown in Fig. 3.9. The “parallel” projection of velocity does not change, as

$$\frac{d\vec{p}_1^b}{dt} = q \frac{\vec{v}_1^b \times \vec{B}}{c} = q \frac{v_1^b \vec{b} \times \vec{B}}{c} = 0 \quad (18)$$

which means that the particle moves uniformly in b -direction. In the plane $(\vec{n}\vec{u})$ the particle gyrates in a perfect circle of radius r_H given by Eq. (2). The instantaneous vector \vec{u} points exactly towards the center o of a planar gyro-orbit (see Fig. 3.9).

During a single time step, τ , a particle makes a rotation through angle φ in the plane $(\vec{n}\vec{u})$ as shown in Fig. 3.9:

$$\varphi = \frac{2\pi q B \tau}{m_0 \gamma c} = \frac{2\pi q B \tau}{\sqrt{m_0^2 c^2 + p^2}} \quad (19)$$

The corresponding rotational transformation is given by

$$\begin{cases} v_2^n = v_1^n \cos \varphi \\ v_2^u = v_1^n \sin \varphi \end{cases} \quad (20a)$$

where we have employed the fact that $v_1^u \equiv 0$ for the coordinate system construction.

Thus, the new particle velocities after rotation in the magnetic field are:

$$\vec{v}_2 = v_1^b \vec{b} + v_1^n \cos \varphi \vec{n} + v_1^n \sin \varphi \vec{u} \quad (20b)$$

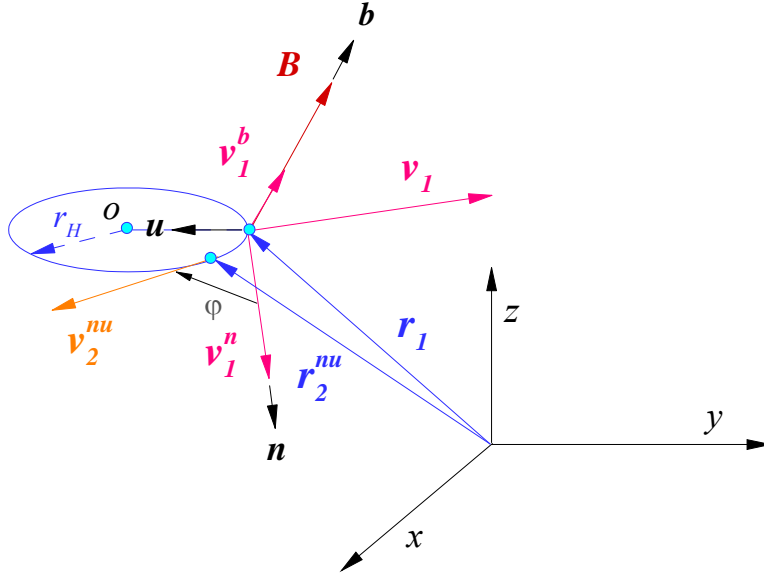


Figure 3.9 - Vectors B -field and velocity, and its parallel and perpendicular projections with respect to the magnetic fields and two coordinate systems.

Next, we have to calculate new spatial position of a particle. The coordinate of the projection on plane $(\vec{n}\vec{u})$ of the center o of the helical trajectory (Fig. 3.9) is:

$$\vec{r}_0 = \vec{r}_1 + r_H \vec{u} \quad (21)$$

Note that in Eq. (21) we assume that the gyro-radius has a sign depending on that of the particle charge. The $(\vec{n}\vec{u})$ projection of the velocity is always tangential to the gyro-orbit. Therefore, it is calculated similar to Eqs. (20ab) as:

$$\vec{r}_2^{nu} = \vec{r}_0 + r_H \cos \varphi \vec{n} - r_H \sin \varphi \vec{u} \quad (22)$$

Finally, the new particle coordinate is calculated as a superposition of uniform parallel and circular perpendicular to the magnetic field motions:

$$\vec{r}_2 = v_1^b \Delta \vec{b} + \vec{r}_2^{nu} \quad (23)$$

Obviously, the particle trajectory is an exact helix, which becomes a straight line in the $\vec{B} \rightarrow 0$ limit, and a perfect circle when $v_1^b \rightarrow 0$.

3.5 Monte-Carlo calculations of radiation flux reduction

We have traced millions of trajectories of the particles with energies from 0 to 100 GeV that have energy distributions as presented in Fig. 3.10. Protons and alpha-particles in this energy range are responsible for the majority of the cosmic ray flux.

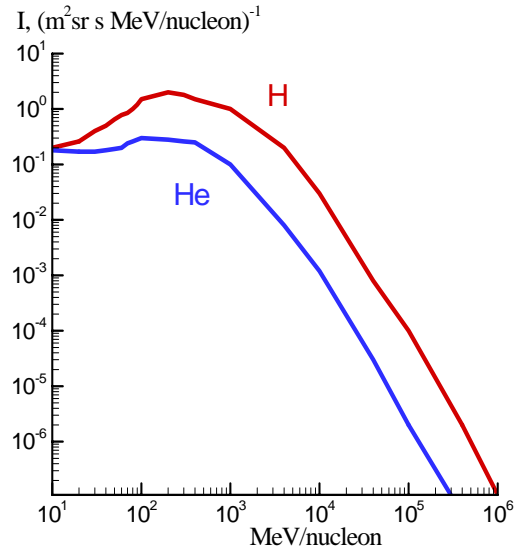


Figure 3.10 – Energy spectrum of cosmic rays as given in the [Particle Data Group, 2004]

The simulation domain is shown in Fig. 3.11. Uniformly along a spherical surface that surrounds the magnetic coil assembly, we continuously simulate impinging particles with the required energy distribution. These particles travel inside the magnetic field domain until they leave it a later moment. The contribution of all particles to the radiative flux and density is periodically accumulated over a long period of time until satisfactory statistical information is gathered. This requires typically 10-100 events per spatial cell.

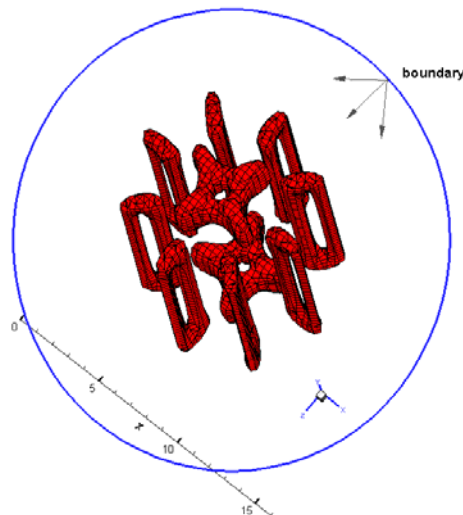


Figure 3.11 – The spherical simulation domain with particle injection from the boundary

The following randomization procedure assuring that we match the experimental cosmic ray fluxes is used. The flux is assumed to be isotropic in space, as is the distribution function of particles, $f(\vec{v}) = f(v)$, which defines the number of particles on the elementary phase space volume as $dN = f(\vec{v})d\vec{v} = f(v)4\pi v^2 dv$. What is actually presented in Fig. 3.10 is the directional particle flux $\int d\Gamma^+ = \int v_x f(\vec{v})d\vec{v}$, which is equal to the flux collected by a plane surface in a second, divided by the solid angle 2π . For a given kinetic energy

$$E = \sqrt{p^2 c^2 + m_0^2 c^4} - m_0 c^2 \quad (24)$$

(with corresponding velocity v) the isotropic distribution is generated using two normal random numbers $\xi_{1,2} \in]0,1[$, which define a random position on a sphere as follows:

$$\begin{cases} v_x = v \sqrt{1 - \mu^2} \cos \varphi \\ v_x = v \sqrt{1 - \mu^2} \sin \varphi, \\ v_z = v\mu \end{cases} \quad \begin{cases} \varphi = 2\pi\xi_1 \\ \mu = 2\xi_2 - 1 \end{cases} \quad (25)$$

here $\mu = \cos \theta$, and $\theta \in [0, \pi]$ and $\varphi \in [0, 2\pi]$ are the spherical coordinates $\{v, \varphi, \theta\}$.

But to proceed with Eq. (25) we have to convert energy dependence of the fluxes to velocity-dependence. In the spherical coordinates a directional particle flux is:

$$\Gamma^+ dv = 2\pi \int_0^1 v \mu f(v) d\mu dv = \pi v f(v) dv \quad (26)$$

which when divided by the half-space solid angle gives $\Gamma^+(v) = 0.5v f(v)$, in accord with the fact that the average projection of a velocity is half of its amplitude. Thus, we have:

$$d\Gamma^+(v) = 0.5v dN = 0.5v(E) f(E) dE \quad (27)$$

We use the following dimensional units in the calculations: proton mass m_p , electron charge e , speed of light in vacuum c , and $E = 1 \text{ GeV}$ for particle energy. Hence, the unit for momentum is $m_p c$, and for time $1m/c$. The dimensionless relation between momentum (velocity) and energy, as well as expressions for gyro-radius Eq. (2) and precession angle Eq. (19) is:

$$\begin{aligned} p &= (1.065E + m)^2 - m^2 \geq 0 \\ v &= \frac{p/m}{\sqrt{1 + p^2/m^2}} < 1 \\ r_H(m) &= 3.13 \frac{p}{qB}, \quad \Delta\varphi = 2 \frac{qB\tau}{m} \end{aligned} \quad (28)$$

The whole interval of energies of interest, $E = 0 - 100 \text{ GeV}$, is divided into ~ 30 bins with $\Delta E \sim 0.1 - 5 \text{ GeV}$ per bin. The total flux carried by particles emitted during a time step τ from a unit area on the boundary surface (Fig. 3.11) for a single bin is:

$$\Delta\Gamma^+ = \Gamma^+ \Delta E \tau = 0.5 \langle v(E) \rangle \Delta N = 0.5 \langle v(E) \rangle K \eta \quad (28)$$

where $\langle v(E) \rangle$ is the mean velocity within the segment, and K is the number of test particles for the bin. Usually this number is fixed for all bins to allow equal relative statistical accuracy. From Eq. (28) we can calculate the weight of a single particle to be:

$$\eta = \frac{2\Gamma^+ \Delta E \tau}{v(E) K} \quad (29)$$

When calculating the actual flux intercepted by a control surface of unit area, the ratio

$$\delta = \frac{\sum_i \eta_i}{\Gamma^+ \Delta E \tau} \quad (30)$$

will give a factor of radiation reduction with respect to the background level.

The results of modeling show that cutting off 95% of particles with $E < 4\text{GeV}$ is achieved with $\langle BL \rangle \sim 10\text{Tm}$. To reduce a radiation flux to 5% of its background value a magnetic field rigidity on the order of 25Tm will be required.

In the following Figs. 3.12a and 3.12b we present results for the 2-magnetic plug configuration, similar to one shown in Fig. 3.11, but with double the number of coils in each group. The three sets of runs have been performed for $\langle BL \rangle \sim 5, 10$, and 25Tm .

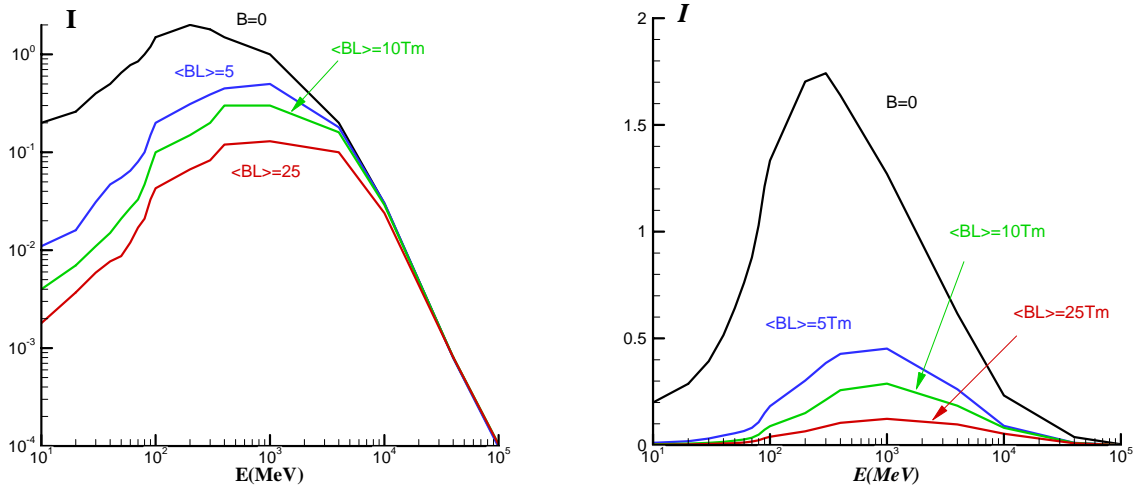


Figure 3.12a – The energy spectrum of protons in the center of the $6\text{m} \times 6\text{m}$ habitat for different various magnetic field rigidities. The left figure has a logarithmic ordinate, while the right one has a linear ordinate.

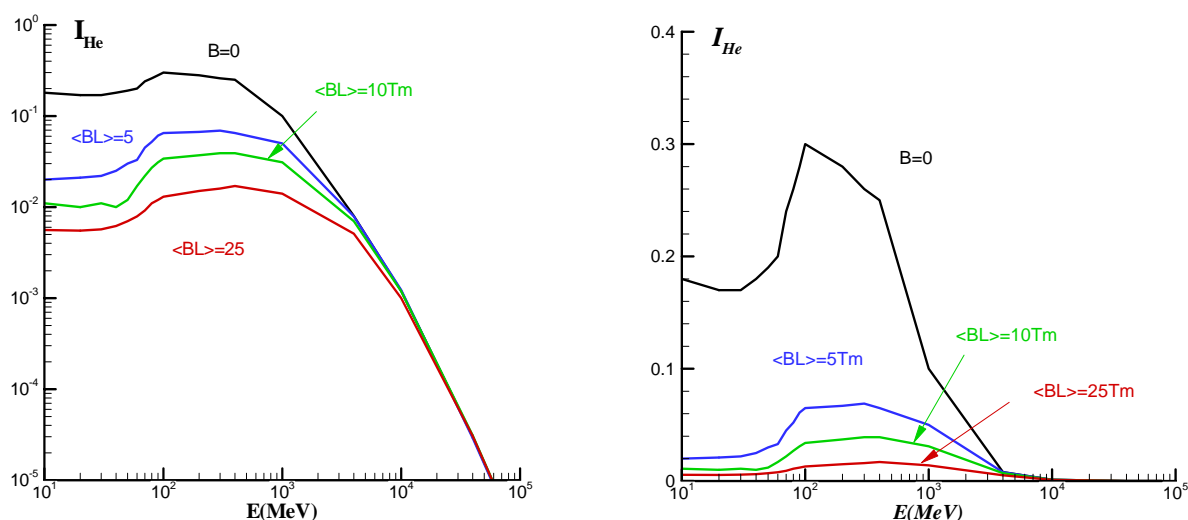


Figure 3.12b – The energy spectrum of alpha-particles penetrating through the 16-coil magnetic shield with $\langle BL \rangle = 5, 10$ and 25 Tm . The left figure has a logarithmic ordinate, while the right one has a linear ordinate.

3.6 Discussion of Results

Even with $\langle BL \rangle$ at the lowest value of 5 Tm , significant particle flux reduction is produced in the $4\text{-}5 \text{ GeV/nucleon}$ energy range, indicating the effectiveness of magnetic shielding for protons and alpha particles, and by extrapolation for heavier particles as well. As mentioned above, we would like to extend these calculations and carry out a full 3-dimensional grid calculation, but we have confidence that the Biot-Savart summation method for the magnetic field gives sufficient accuracy to provide confidence in the results presented here.

4. Design considerations for a real superconducting magnetic shield system

Given the encouraging results shown above, we now look briefly at the engineering challenges that must be faced if a real superconducting magnetic shield is to be built. As noted in our proposal, the bulk of the engineering analysis was planned to be performed in Phase II.

A practical magnetic shield will need a coil system with mechanical support as well as control and cooling systems. Assessing the practicality of the system we have analyzed above requires some idea of the weight, power consumption and amount of helium coolant. The stored energy and internal mechanical forces also need assessment. For this study, we scale from the AMS cryomagnet, currently under construction at Space Cryomagnetics in Cullum, England. [AMS Collaboration, 2004]

The AMS cryomagnet has the following characteristics:

- A central field of 0.9 T
- A bending power 0.8 Tm^2 is over a volume of 0.7m^3 .
- The heat load is about 10 W
- 2500 l (312 kg) of liquid helium will be carried.
- 5.5 MJ is stored in the magnetic field.
- A coil mass of roughly 1000 kg and a total mass of roughly 2357 kg.
- A power consumption of 700 W to power four cryocoolers

Based on scaling, we can make some rough estimates of the characteristics of the magnetic shield we have described above. We start with the weight: assuming a density of 5 g/cm^3 for the coil conductor, the total mass of the coils will be 244 tons. For the AMS cryomagnet, the coils constitute 61% of the total mass of 2357 kg and applying factor gives a total mass of 395 tons for the magnetic shield.

This estimate is grossly naïve: the forces between the coils are proportional to the square of the magnetic field and the strength of the support structure goes like the cross sectional area; the support structure would need to be much thicker. Based on the analysis above, the scale size of the support increases by a linear factor $L = \sqrt[3]{395t/2.3t} = 5$, so the cross sectional area of the support members increases like $L^2 = 25$. In order to support the increased magnetic field, the cross sectional area need to increase by a factor of 100, so an additional factor of four is required, so using this scaling gives a total mass of 1600 t. Using advanced materials with greater strength-to-weight ratios (such as carbon nanotube-based fibers) would reduce the required support mass.

The total amount of helium required and the cooling power may be estimated in two ways. First, if we assume the heat load comes from radiative transfer, the heat load would be roughly proportional the surface areas of the coils, giving a heat load of 2.4 kW for the magnetic shield. Assuming the same factors apply, this translates to 75 tons of liquid helium for a three year mission and a cryocooler power requirement of 169 kW.

The AMS cryomagnet cold mass is supported by sixteen straps which could cause heat to enter by conduction. The amount of heat which enters is proportional to the cross sectional area of the straps, as is their support strength. Thus, the heat load should be proportional to the coil mass, giving a heat load of 1.7 kW, which would require 52 t of liquid helium and 117 kW of cryocooler power.

A challenge to any design will be the ability to dissipate power in the case of a quench. For AMS, the 5.5 MJ of stored energy may be dumped to the support structure which weighs about 1500 kg. The temperature rise is about 30 C. For the magnetic shield, the total stored energy is 16 GJ which would require a dump mass of almost 5000 tons for the same temperature rise.

In summary, the magnetic shield will:

- reduce the total radiation dose by a factor of at least three in a 200 m^3 habitable volume
- have a mass of between 400 and 1600 t
- require 52-75 tons of liquid helium for a three year mission
- need 117-169 kW of power for cryocoolers
- store 16 GJ of energy, requiring a dump mass of 5000 tons for a 30 C temperature increase

5. Summary of calculations and further directions for research

Clearly, the construction of the magnetic shield we have described constitutes a massive undertaking, and our study points out several challenges. As a next step, a complete calculation of the dose reduction needs to be carried out, including interactions of the incident particles with the coils and support structure. Secondary particles, neutrons in particular, could pose a serious background threat. In our preliminary calculation, we made no comparison with passive shielding, and a detailed comparison must be made, preferably with the same code.

Our design would effectively shield a crew from cosmic radiation during a three-year deep space voyage, and this motivated our choice of baseline parameters. The design certainly could be optimized for weight reduction. For example, the weight of the support structure scales very roughly with B^2 and linearly with L . Reducing the field by 10% while increasing L by 7% would keep the same reduction while reducing the mass by 13%. Further, one end of the habitat will be connected to the spacecraft services, so a coil system at that end will not be needed, reducing the mass by 20-25%. Also, the number and geometry of the coils could be optimized, resulting in further savings.

In doing this optimization, we propose to use the most realistic analytical model possible of the magnetic field configuration, so as to maintain confidence in our predictions. We plan to develop an advanced 3D3V kinetic model, which will allow accurate resolution of coils and structure by utilizing a non-uniform, unstructured grid. Next, some of the important processes such as the production of secondary particles via collisions of cosmic ray particles with structural elements will be included into the computational model. We will perform predictive calculations using data for realistic operational superconducting magnetic systems


Finally, many of our arguments above are based on scaling laws motivated by simple physical ideas, but generally naïve. A detailed study of the scaling of the various AMS systems to the size we propose needs to be undertaken. In summary, we have established the basic range of parameters of *an example* of a magnetic shield which would suffice for a Mars mission. Further detailed study will determine the practicality of such a system.

6. Media Interest and Outreach

6.1 External Interest in this Research

It is apparent that many science writers look at NIAC announcements. Since the awarding of our Phase I study contract, we have had over a dozen requests for interviews about the work, leading to articles in newspapers, journals and the web. We reproduce one example below, [Universe Today, 18 November, 2004]:

Universe Today - Magnetic Bubble Could Protect Astronauts on Lo... http://www.universetoday.com/am/publish/magnetic_bubble_protect...



UNIVERSE
T O D A Y

Space News from Around the Internet
Updated Every Weekday

Google

NEWS ARCHIVE TOPICS FORUM PHOTOS LINKS

Web www.universetoday.com

[Magnetic Therapy™ from](#)
Magnetic Therapy Ltd - The Company
Free & Fast Global Delivery

[Energy For Life](#)
With Pulsed Magnetic Fields Only 15
minutes a day!

[Magnetic Field](#)
Yahoo! Shopping: Compare & Save
Top brands, great stores, low price

[Magnets work. Now try](#)
"A Significant Breakthrough"
Alternative Medicine Magazine

Magnetic Bubble Could Protect Astronauts on Long Trips

Summary - (Nov 17, 2004) It's the year 2027 and NASA's Vision for Space Exploration is progressing right on schedule. The first interplanetary spacecraft with humans aboard is on course for Mars. However, halfway into the trip, a gigantic solar flare erupts, spewing lethal radioactive protons directly at the spacecraft. But, not to worry. Research by former astronaut Jeffrey Hoffman and a group of MIT colleagues back in the year 2004 ensured that this vehicle has a state-of-the-art superconducting magnetic shielding system that protects the human occupants from any deadly solar emissions.

Full Story - New research has recently begun to examine the use of superconducting magnet technology to protect astronauts from radiation during long-duration spaceflights, such as the interplanetary flights to Mars that are proposed in NASA's current Vision for Space Exploration.

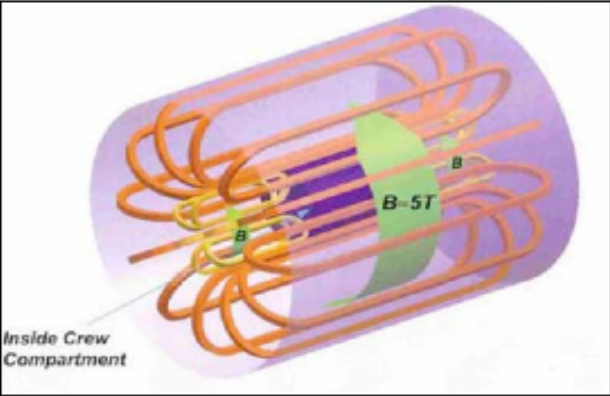
The principal investigator for this concept is former astronaut Dr. Jeffrey Hoffman, who is now a professor at the Massachusetts Institute of Technology (MIT).

Hoffman's concept is one of 12 proposals that began receiving funding last month from the NASA Institute for Advanced Concepts (NIAC). Each gets \$75,000 for six-months of research to make initial studies and identify challenges in developing it. Projects that make it through that phase are eligible for as much as \$400,000 more over two years.

The concept of magnetic shielding is not new. As Hoffman says, "The Earth has been doing it for billions of years!" Earth's magnetic field deflects cosmic rays, and an added measure of protection comes from our atmosphere which absorbs any cosmic radiation that makes its way through the magnetic field. Using magnetic shielding for spacecraft was first proposed in the late 1960's and early 70's, but was not actively pursued when plans for long-duration spaceflight fell by the wayside.

However, the technology for creating superconducting magnets that can generate strong fields to shield spacecraft from cosmic radiation has only recently been developed. Superconducting magnet systems are desirable because they can create intense magnetic fields with little or no electrical power input, and with proper temperatures they can maintain a stable magnetic field for long periods of time. One challenge, however, is developing a system that can create a magnetic field large enough to protect a bus-sized, habitable spacecraft. Another challenge is keeping the system at temperatures near absolute zero (0 degrees Kelvin, -273 C, -460 F), which gives the materials superconductive properties. Recent advances in superconducting technology and materials have provided superconductive properties at higher than 120 K (-153 C, -243 F).

There are two types of radiation that need to be addressed for long-duration human spaceflight, says William S. Higgins, an engineering physicist who works on radiation safety at Fermilab, the particle accelerator near



Inside Crew
Compartment

Image credit: MIT

SUBSCRIBE FREE!

Email:

[Join](#)

[More newsletters](#) (text, weekly edition, etc)

25,000 subscribers and growing.


XML Version [XML](#)

SUPPORT UNIVERSE TODAY

Help me maintain and improve Universe Today.

[Make a Donation](#)

SPONSOR



The second page of the above article follows below:

Chicago, IL. The first are solar flare protons, which would come in bursts following a solar flare event. The second are galactic cosmic rays, which, although not as lethal as solar flares, they would be a continuous background radiation to which the crew would be exposed. In an unshielded spacecraft, both types of radiation would result in significant health problems, or death, to the crew. The easiest way to avoid radiation is to absorb it, like wearing a lead apron when you get an X-ray at the dentist. The problem is that this type of shielding can often be very heavy, and mass is at a premium with our current space vehicles since they need to be launched from the Earth's surface. Also, according to Hoffman, if you use just a little bit of shielding, you can actually make it worse, because the cosmic rays interact with the shielding and can create secondary charged particles, increasing the overall radiation dose. Hoffman foresees using a hybrid system that employs both a magnetic field and passive absorption. "That's the way the Earth does it," Hoffman explained, "and there's no reason we shouldn't be able to do that in space."

One of the most important conclusions to the second phase of this research will be to determine if using superconducting magnet technology is mass effective. "I have no doubt that if we build it big enough and strong enough, it will provide protection," Hoffman said. "But if the mass of this conducting magnet system is greater than the mass just to use passive (absorbing) shielding, then why go to all that trouble?". But that's the challenge, and the reason for this study. "This is research," Hoffman said. "I'm not partisan one way or the other; I just want to find out what's the best way." Assuming Hoffman and his team can demonstrate that superconducting magnetic shielding is mass effective, the next step would be doing the actual engineering of creating a large enough (albeit lightweight) system, in addition to the fine-tuning of maintaining magnets at ultra-cold superconducting temperatures in space. The final step would be to integrate such a system into a Mars-bound spacecraft. None of these tasks are trivial. The examinations of maintaining the magnetic field strength and the near-absolute zero temperatures of this system in space is already occurring in an experiment that is scheduled to be launched to the International Space Station for a three-year stay. The Alpha Magnetic Spectrometer (AMS) will be attached to the outside of the station and search for different types of cosmic rays. It will employ a superconducting magnet to measure each particle's momentum and the sign of its charge. Peter Fisher, a physics professor also from MIT works on the AMS experiment, and is cooperating with Hoffman on his research of superconducting magnets. A graduate student and a research scientist are also working with Hoffman.

NIAC was created in 1998 to solicit revolutionary concepts from people and organizations outside the space agency that could advance NASA's missions. The winning concepts are chosen because they "push the limits of known science and technology," and "show relevance to the NASA mission," according to NASA. These concepts are expected to take at least a decade to develop.

Hoffman flew in space five times and became the first astronaut to log more than 1,000 hours on the space shuttle. On his fourth space flight, in 1993, Hoffman participated in the first Hubble Space Telescope servicing mission, an ambitious and historic mission that corrected the spherical aberration problem in the telescope's primary mirror. Hoffman left the astronaut program in 1997 to become NASA's European Representative at the US Embassy in Paris, and then went to MIT in 2001. Hoffman knows that to make a space mission possible, there's a lot of idea development and hard engineering which precedes it. "When it comes to doing things in space, if you're an astronaut, you go and do it with your own hands," Hoffman said. "But you don't fly in space forever, and I still would like to make a contribution." Does he see his current research as

important as fixing the Hubble Space Telescope? “Well, not in the immediate sense,” he said. “But on the other hand, if we ever are going to have a human presence throughout the solar system we need to be able to live and work in regions where the charged particle environment is pretty severe. If we can’t find a way to protect ourselves from that, it will be a very limiting factor for the future of human exploration.”

Written by [Nancy Atkinson](#)

6.2 Presentation to the physics community

In addition to the media interest described above, we want to present our NIAC research to the broader physics community to elicit their comments and interest. We presented the following poster at the meeting of the American Physical Society in Savannah in November, 2004. [Fisher, et. al. 2004]:

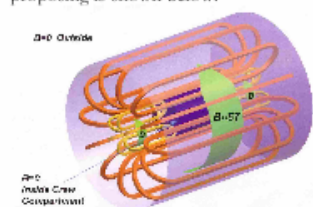
NM2B.010 **Superconducting Magnet Shielding of Astronauts from Cosmic Rays**

P. Fisher, J. Hoffman, F. Zhou, O. Batishchev

Massachusetts Institute of Technology, Cambridge, USA

Radiation has long been recognized as one of the most serious health problems facing astronauts exploring space beyond the Earth's magnetic shield. (Townsend, 2000) Surrounding a cylindrical habitable volume of 2.5 m diameter and 3.5 m length with enough aluminum to absorb protons with kinetic energies less than E_k is given by $M(kg) = E_k(MeV)^{1.67}$; to stop protons with energies less than 1.2 GeV requires 139 metric tons of shielding. No matter what improvements are made in the efficiency of in-space propulsion systems, the cost of getting enough propellant into low Earth orbit to carry this amount of “dead mass” to Mars and back will be huge. Using liquid hydrogen as a shielding material can somewhat reduce the required mass, but the required shielding mass is still extremely large. Magnetic shielding relies on the bending of charged particles passing through a magnetic field to protect an internal volume from incident cosmic radiation. (The Earth's magnetic field accomplishes this for astronauts in low Earth orbit.) For a magnetic field of strength B and width w , protons of momentum $p(GeV) \sim 0.3 B(T) w(m)$ are bent away. A one-meter wide

region of 5T magnetic field would exclude protons with kinetic energy below 1.5 GeV, ensuring the same protection as ~ 1.7 m of aluminum absorber. The mass of the magnetic system, however, would be between one and two orders of magnitude less than the mass of an equivalent aluminum shield. Attaining large magnetic fields over large volumes requires superconducting magnets. Recent advances in superconducting magnet design have made such a system feasible. The notional geometric configuration of the magnetic shielding system we are proposing is shown below.

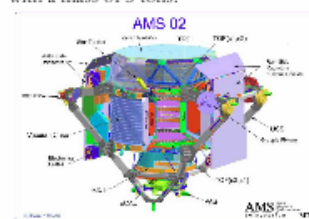


Requirements for such a magnet include:

- Low external field - < 60 G
- Long endurance - 3 y
- Stability
- Efficient geometry

This is very similar to VASIMR and other advanced RF-driven thrusters.

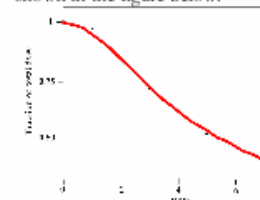
The superconducting cryomagnet for the Alpha Magnetic Spectrometer (AMS) experiment represents an exciting step toward the practical possibility of realizing a magnetic shield. The AMS design meets the requirements above for a 1 m³ volume with a mass of 3 tons.



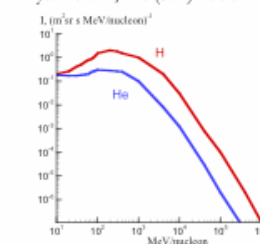
Our NAIC Phase I study centers on

- Optimizing field and coil design
- Studying key technologies which will need to be scaled up, including
 - High power cryocoolers
 - Gorter-Mellink heat transfer systems
 - Bilinear supports for the cold mass
 - Quench protection and control
- Calculation of dose reduction for comparison with conventional absorber systems.

Our first calculation for reduction of dose by a magnetic shield indicates an achievable field of 7-10 T reduce the radiation dose to industrially acceptable level shown in the figure below.



Cosmic ray flux I is taken from published experimental data: Review by Particle Data Group Phys. Lett. B, 1-4 (592) 2004.



Next step includes 3D geometrical models of magnets, cryocoolers and payload. We will address secondary production and synergy with plasma propulsion schemes using high magnetic fields.

The final results will be presented at the MIT-NASA Radiation Shielding Workshop, Cambridge, MA, 13-14 June, 2005.

References

Letaw, J., R. Silberberg and C. Tsao, Nature, **330**, 709, 1987.

Spillantini, P., F. Taccetti, P. Papini and L. Rossi, Nucl. Inst. Meth. A **443**, 254, 2000.

Particle Data Group, Review of Particle Physics, Phys. Lett. B, 1-4 (**592**) 1-1109, 2004.

Landis, G.A. "Magnetic radiation shielding: an idea whose time has returned?", 10th Biennial SSI/Princeton Conference on Space manufacturing, Princeton, NJ, May 15-19, 1991.

Townsend, L.W. "Overview of active methods for shielding spacecraft from energetic space radiation", 11th Annual NASA Space Radiation Health Investigator's Workshop, Arona (Italy), May 27-31, 2000.

AMS Collaboration, submitted to Nucl. Inst. Meth., 2004.

Batishchev, O.V. et al, "Unstructured adaptive grid and grid-free methods for magnetized plasma fluid simulations", J. Plasma Phys. **61**, part 5, 701, 1999.

Batishchev, O. et al, "2.5D Adaptive Mesh PIC-Vlasov Hybrid Method for Laser-Matter Interactions in the Presence of Strong Gradients", p.387, 18th ICNSP, Cape Cod, 7-10 September, 2003.

Fisher, P., J. Hoffman, F. Zhou, O. Batishchev, "Superconducting Magnet Shielding of Astronauts from Cosmic Rays", APS Bulletin, **49** (8) 261, November 2004.